Since January 2020 Elsevier has created a COVID-19 resource centre with free information in English and Mandarin on the novel coronavirus COVID-19. The COVID-19 resource centre is hosted on Elsevier Connect, the company's public news and information website.

Catena 223 (2023) 106924

Contents lists available at ScienceDirect

Catena

journal homepage: www.elsevier.com/locate/catena

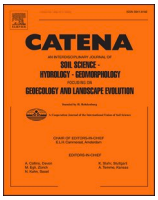

Mapping abandoned cropland using Within-Year Sentinel-2 time series

Bo Liu [a,b], Wei Song [a,c,*]

[a] Key Laboratory of Land Surface Pattern and Simulation, Institute of Geographic Sciences and Natural Resources Research, Chinese Academy of Sciences, Beijing 100101, PR China
[b] School of Geomatics, Liaoning Technical University, Fuxin 123000, PR China
[c] Hebei Collaborative Innovation Center for Urban-rural Integration development, Shijiazhuang 050061, PR China

ARTICLE INFO

Keywords:
Food security
Change detection within-year
Time series
Land use mapping
GEOBIA
Linxia County

ABSTRACT

Against the background of the COVID-19 pandemic and various armed conflicts, the world is experiencing an unprecedented food crisis. The reclamation of abandoned cropland with food production potential may increase the global food supply in a short period of time, ensuring food security. At present, the extraction of abandoned cropland is mainly based on low- and medium-resolution remote sensing image data, making it difficult to extract fragmented areas in mountainous regions and to distinguish between abandoned cropland and transitional classes (such as fallow cropland). We developed a change-detection method based on within-year Sentinel-2 time series to extract cropland abandoned from 2018 to 2021 and defined four types of croplands, namely spontaneously abandoned, induced abandoned, fallow, and lost cropland, using Linxia County in mountainous China as the study region. First, cropland objects were generated from multi-temporal Sentinel-2 images using the multi-resolution segmentation method, and the land use map of Linxia County from 2017 to 2021 was drawn using random forest classifier. Second, through defining and identifying different cropland types, the interannual dynamic changes in cropland from 2018 to 2021 were extracted by analyzing the annual land use change trajectory. Third, by analyzing the normalized difference vegetation index (NDVI) time series of cropland within-year, the active and cultivated cropland sites within-year were extracted by threshold segmentation. Finally, the changes in the four cropland types were extracted by intersecting the two result types. Our method captured the object level changes well (overall mapping accuracy = 93 ± 5 %), and the extraction accuracy of abandoned cropland reached 81 ± 2 %. Abandoned cropland was mostly located in areas of medium quality and with a moderate distance from rural settlements. Reclamation can potentially increase the grain production in Linxia County by at least 3.6 % and needs to be combined with the local natural geography and human activities. Our method is a robust method for extracting abandoned cropland and may be applied to other research related to land use change.

1. Introduction

Against the background of a growing world population and dietary changes, the demand for agricultural products to meet the supply of food, animal feed, fiber, and fuel is increasing (Alexander et al., 2015; Kim et al., 2016). The global demand for food is expected to double by 2050 (Tilman et al., 2011; Tilman and Clark, 2014; Kehoe et al., 2017). In recent years, the impacts of the COVID-19 pandemic and armed conflicts on global food security have become an issue of high concern. Many countries banning or restricting food exports have intensified inflation, with disastrous impacts on maintaining global livelihood and stability (Carducci et al., 2021; di Caracalla, 2022; Pörtner et al., 2022; Tollefson, 2022). Pandemics and wars have exposed the fragility of food systems and show the urgent need for countries to secure immediate food supplies (Dasgupta and Robinson, 2022). The reclamation of abandoned cropland is a potential option to rapidly increase grain production in the short term, thereby minimizing risks to food security (Gelfand et al., 2013; Schierhorn et al., 2013; Zumkehr and Campbell, 2013; Field et al., 2020), which is of great significance to solve the current global food crisis.

Information about abandoned cropland is mostly acquired through farmer surveys. The largest advantage of this method is that it can

* Corresponding author at: Key Laboratory of Land Surface Pattern and Simulation, Institute of Geographic Sciences and Natural Resources Research, Chinese Academy of Sciences, 11A, Datun Road, Chaoyang District, Beijing, 100101, People's Republic of China.
E-mail address: songw@igsnrr.ac.cn (W. Song).

https://doi.org/10.1016/j.catena.2023.106924
Received 28 July 2022; Received in revised form 8 December 2022; Accepted 3 January 2023
Available online 11 January 2023

explain the mechanism behind cropland abandonment (Li et al., 2014), although it lacks spatial details, making it difficult to obtain a complete view of all abandoned cropland areas within a given study region (Yan et al., 2016; Li et al., 2017; Kuntz et al., 2018). With the emergence of multiple sensors with different imaging scales, resolutions, and ranges, remote sensing (RS) has been widely recognized as an effective tool to detect the spatial and temporal dynamic distribution of abandoned cropland with less time, lower costs, better accuracy, and higher coverage (Estel et al., 2015; Yin et al., 2018a, 2020). At present, the methods of extracting abandoned cropland based on remote sensing data mainly include the normalized difference vegetation index (NDVI) time series change detection method and the inter-annual land use change detection method. The first method mainly uses NDVI time series of high time resolution data, such as AVHRR, MODIS, and SPOT VEGETATION data, to extract abandoned cropland (Campbell et al., 2008; Siebert et al., 2010; Alcantara et al., 2013; Estel et al., 2015). For example, Estel et al. (2015) extracted the abandoned cropland in Europe using time-series MODIS satellite data and drew a map of the reclamation extent of abandoned cropland. The advantage of this method is that it can rely on the satellite's high time resolution and long life and can capture seasonal-to-decade cropland abandonment dynamics, but the spatial resolution is low (1 km to 250 m). For cropland with relatively a high fragmentation degree (Kuemmerle et al., 2013; Hartvigsen, 2014), the classification results may be less reliable. Compared with low-resolution satellite data, medium-resolution Landsat images (30 m) can monitor abandoned cropland at a more refined spatial scale (Duveiller and Defourny, 2010; Blair et al., 2018), which greatly improves the accuracy of abandoned cropland extraction.

Recently, an inter-annual land use change detection method for mapping abandoned cropland using annual Landsat time series data during the study period has emerged (Romero and Perry, 2004; Baumann et al., 2011). For example, Song (2019) mapped different types of abandoned cropland in mountain areas of China by monitoring Landsat and HJ-1 satellite images and applying the successive annual land use changes from 2012 to 2017. Dara et al. (2018) used the time series of Landsat images and, based on the random forest classification method, extracted cropland abandoned in northern Kazakhstan from 1988 to 2013. The advantage of this method is that it can identify the change characteristics of abandoned cropland in a certain period, but the extraction accuracy is greatly affected by the initial land use classification accuracy, which is prone to error transfer (DeVries et al., 2015; Yin et al., 2018a; Wang and Song, 2021).

The inter-annual land use change detection method can be used on pixels or image objects. In practice, pixel-based classification results inevitably cause "salt and pepper noise". Yin et al. (2020) selected 14 study regions globally, using the Landsat time series to map the extent and time of cropland abandonment and to distinguish among stable, abandoned, and fallow cropland. However, in some mountainous areas, most pixels are a mixture of cropland as well as herbaceous and woody plants, and abandoned cropland in these areas is difficult to map due to the effect of mixed pixels (Miller et al., 2017). In Asia and Africa, most agricultural systems belong to small groups of farmers, and pixel-based studies often fail to depict individual cropland (Xiong et al., 2017). The Geographic Object-based Image Analysis (GEOBIA) (Sitokonstantinou et al., 2018; Feizizadeh et al., 2021; Janowski et al., 2021; Oreti et al., 2021) delineates any analysis unit by segmenting the image; the image information is closer to the features of the real world (Whiteside et al., 2011), with a higher classification accuracy and application potential than pixel-based methods in land cover mapping and change detection (Im et al., 2008; Stow et al., 2008; Inglada et al., 2015; Lebourgeois et al., 2017). This is therefore an effective method to improve the accuracy of land use classification. At present, the analysis of abandoned cropland is mainly focused on pixel-level algorithms, and studies on the object-based extraction of abandoned cropland are scarce (Yin et al., 2018b).

Although inter-annual change detection methods are increasingly used to monitor cropland abandonment at medium and high spatial resolution scales, they are only based on one or more pairs of images before and after change, and the classification processes of heterogeneous images are independent of each other, which easily ignores vegetation changes in the growth cycle. However, the time resolution of Landsat images is as low as 16 days, making it difficult to find sufficient cloud-free images in appropriate periods to establish long time series NDVI data covering different crop growth periods. Compared with Landsat data, Sentinel-2A/B data with a spatial resolution of 10 m and a revisit period of only 5 to 10 days offer an unprecedented opportunity for global agricultural monitoring (Battude et al., 2016; Drusch et al., 2012; Matton et al., 2015; Valero et al., 2016), providing more spatial details and a higher temporal resolution (Lebourgeois et al., 2017, Sitokonstantinou et al., 2018). Previously, Sentinel-2 data have been used for crop classification (Belgiu and Csillik, 2018; Van et al., 2018), estimations of chlorophyll and nitrogen contents of crops (Clevers and Gitelson, 2013; Herrmann et al., 2011), delineations of cropland boundaries (Xiong et al., 2017), and crop yield prediction (Jin et al., 2019), among others. However, there are few studies that prove the potential of Sentinel-2 time series data in the extraction of abandoned cropland (He et al., 2022).

In this context, this paper develops a new method for extracting abandoned cropland within-year by combining the NDVI time series of Sentinel-2 remote sensing images with the annual land use trajectory of the object level. Two types of cropland abandonment, spontaneous and induced abandonment, were defined, and abandoned cropland was separated from fallow cropland and lost cropland. Linxia County, Gansu Province, China, was used as the research area, and we applied Sentinel-2 time-series images from 2017 to 2021 to draw a map of fragmented and abandoned cropland areas in mountainous areas. The research objectives are as follows: 1) To develop a method to identify the abandoned cropland within-year; 2) to identify the distribution of abandoned cropland in Linxia County from 2018 to 2021 and distinguish the cropland types; 3) to analyze the spatial change characteristics of abandoned cropland in Linxia County and to put forward suggestions for reclamation.

2. Research area and data sources

2.1. Overview of the research area

Linxia County (Fig. 1) is under the jurisdiction of Linxia Hui Autonomous Prefecture, Gansu Province, China, and covers a total area of 1,212.4 k m^2. It is in the transition zone between the Qinghai-Tibet Plateau and the Loess Plateau. The landform is mainly mountainous and hilly, with numerous gullies, tablelands, and streams. The terrain is low in the northeast and high in the southwest, with an elevation of 1,697–4,561 m. Linxia County belongs to the transition zone between the temperate semi-humid and alpine humid area, and the climate is semi-humid climate. Because of the characteristics of continental and monsoon mountain climates, the climate factors change with the height of the terrain. The climate is mild in spring and cool and humid in autumn, without heat in summer and severe cold in winter. The average annual temperature is 5.9℃, with an average annual frost-free period of 148 days. The average annual precipitation is 630.6 mm, with an average annual evaporation of 541.9 mm. According to the FAO-90 soil classification system (HWSD, 2009), cambisols is the main soil type in Linxia County, followed by chernozems; phaeozems are less frequent. The soil texture is mainly loam, including loamy sand and silt loam. The dominant harvesting system is one cropping a year, and the main crops include wheat, corn, rapeseed, and potatoes.

Restricted by landform conditions, Linxia County is characterized by water resources shortages, an unbalanced spatial and temporal distribution, structural contradictions of supply, and an ecologically fragile area with fragmented terrain, ravines, and serious soil erosion. The economic aggregate is small, with a low per capita income, an unstable

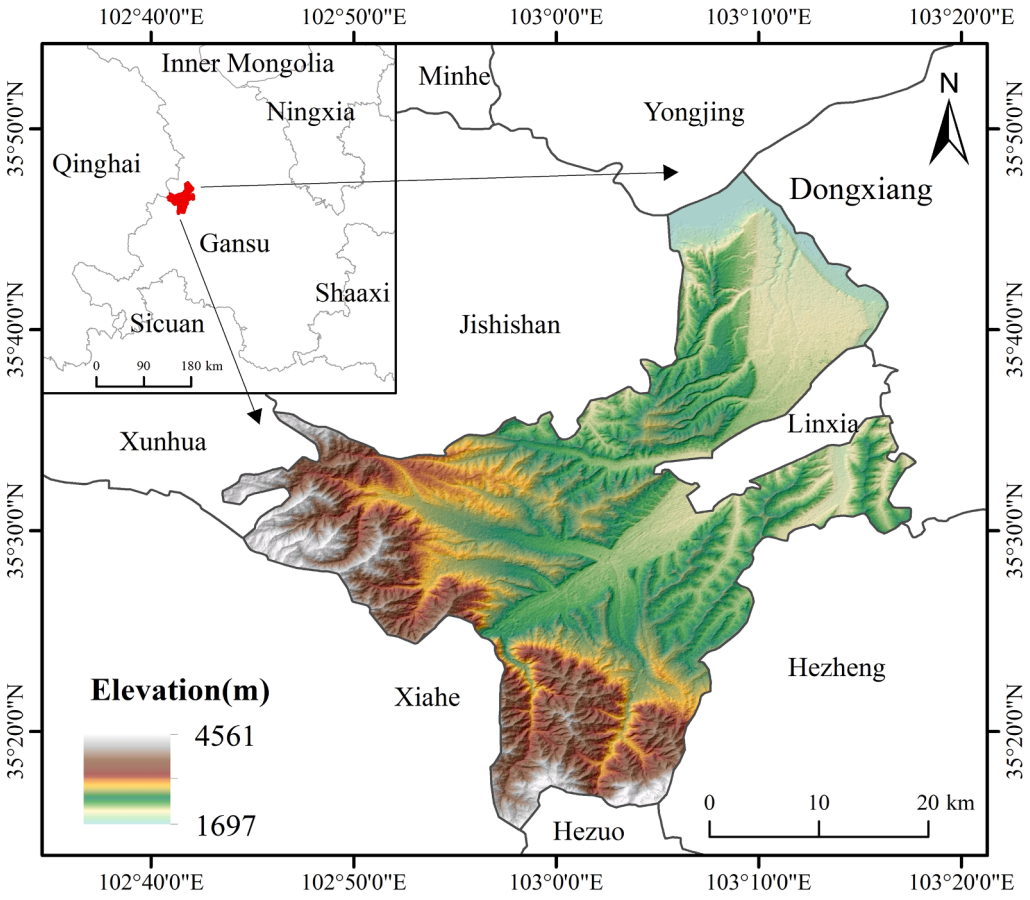

Fig. 1. Geographic Location of Linxia County, Gansu Province, China.

agricultural foundation, rural population outflow, and policy factors that have led to the aggravation of cropland abandonment. In recent years, in an effort to curb cropland abandonment and ensure food production safety, the local government has vigorously pursued the renovation and restoration of abandoned cropland (Linxia County People's Government Network, 2021). On the other hand, a large-scale project to return cropland to forest and grassland was initiated in areas unsuitable for cultivation to mitigate land degradation caused by soil erosion (Linxia Hui Autonomous Prefecture People's Government Network, 2021).

2.2. Data sources

2.2.1. Remote sensing image data

Sentinel-2A/B satellite images with cloud cover less than 20 % were used for 22 days from April 1, 2017, to November 31, 2021; the research area covered two images with a total of 44 periods of data from the European Space Agency (ESA, 2021) (Table 1). Among them, the data in 2017 and 2018 were L1C-level images, which were not atmospherically corrected, only orthorectified and geometrically corrected. The image data from 2019 to 2021 belonged to the L2A level, adding the atmospheric correction link as atmospheric bottom layer reflectivity products.

2.2.2. Other data

We used the 30-m land use and land cover change (LUCC) data from the Chinese Academy of Sciences in 2015, 2018, and 2020 as a reference for delineation samples (RESDC, 2020). These data were constructed based on expert knowledge by using Landsat 8 satellite remote sensing data and human–computer interactive visual interpretation, with an overall accuracy between 83 % and 96 % (Liu et al., 2014). The categories of rural settlements included in the data can be used to understand abandoned cropland at different distances from rural settlements in Linxia County. Google Earth Image (Image Elevation Download Expert, 2021) with a spatial resolution of 0.49 m was used to assess the accuracy of the land-use classification and abandoned cropland maps evaluated by visual discrimination. Digital Elevation Model (DEM) data (30 m) were obtained from the Geospatial Data Cloud Platform (GDC, 2021) and used to calculate the abandonment rate of Linxia County plots under different slopes. Traffic and road data were from the Open Street Map (OSM, 2021) and used to understand the influence of the distance between cropland and roads on cropland abandonment. China's cropland production potential dataset was obtained from the Resource and Environmental Science and Data Center, Chinese Academy of Sciences (RESDC, 2017); it was calculated based on the Global Agro-Ecological Zones (GAEZ) model jointly developed by the Food and Agriculture Organization of the United Nations (FAO) and the International Institute for Applied Systems Analysis IIASA (Fischer et al., 2006; Liu et al., 2015) and used to assess the grain production potential of abandoned farmland after reclamation.

3. Research methods

We mapped cropland abandonment using Sentinel-2 imagery from 2018 to 2021. The workflow of mapping abandoned cropland mainly included the following steps (Fig. 2): First, the Sentinel-2 data were preprocessed. Second, multi-resolution segmentation and random forest classifier in eCognition were used to generate the land use map for 2017–2021, with the aim to estimate the cropland boundaries within-year and to determine the annual land use trajectory of the study area. To improve the accuracy of the classification results, according to the phenological information of crops in Linxia County, the images from

Table 1
Technical details of satellite images for Linxia County.

Acquisition date	Satellite mission and instrument	Processing level	Cloud cover (%)
30 May 2017	S2A_MSI	L1C	4/3
29 July 2017	S2A_MSI	L1C	6/2
12 October 2017	S2B_MSI	L1C	5/3
20 April 2018	S2B_MSI	L1C	9/17
23 August 2018	S2A_MSI	L1C	2/4
12 October 2018	S2A_MSI	L1C	0/1
10 April 2019	S2A_MSI	L2A	3/2
25 April 2019	S2B_MSI	L2A	0/2
20 May 2019	S2A_MSI	L2A	2/2
24 June 2019	S2B_MSI	L2A	2/5
04 July 2019	S2B_MSI	L2A	1/4
29 July 2019	S2A_MSI	L2A	0/1
03 August 2019	S2B_MSI	L2A	4/0
27 September 2019	S2A_MSI	L2A	0/2
17 October 2019	S2A_MSI	L2A	0/1
01 November 2019	S2B_MSI	L2A	1/12
29 April 2020	S2B_MSI	L2A	3/5
28 June 2020	S2A_MSI	L2A	8/5
21 October 2020	S2A_MSI	L2A	0/4
29 April 2021	S2A_MSI	L2A	0/0
13 July 2021	S2B_MSI	L2A	2/3
05 November 2021	S2A_MSI	L2A	0/2

Notes: The whole territory of Linxia County is spliced by two Sentinel-2 satellite images. Table 1 includes 44 images of Linxia County, Gansu Province, China, taken at different 22 days from 2017 to 2021. The satellite mission and instrument and processing levels of the two images are the same on the same day, and the cloud cover of 4/3; 6/2… means that the cloud cover of the two images taken in a day was 4 % and 3 %; 6 % and 2 %, … respectively.

October of each year were selected for classification. Third, the NDVI time series data of cropland within-year were created, and the spatial distribution of planted cropland and uncultivated land was obtained by threshold segmentation. Spontaneous abandonment, induced abandonment, fallow cropland, and lost cropland were distinguished by establishing the identification rules of different cropland types. Finally, the recall rate was used to verify the accuracy of the abandoned cropland maps.

3.1. Data Pre-processing

To ensure consistency across sensors and days, we used the Sen2Cor tool in the Sentinels Application Platform (SNAP, 2019) toolbox for atmospheric correction of Sentinel-2 images to convert the Class 1C Top of Atmosphere (TOA) reflectance product to Class 2A Bottom of Atmosphere (BOA) (Drusch et al., 2012; Muller-Wilm et al., 2013). Three visible bands (red, green, and blue), three red-edge bands (red-edge 705, 740, and 783), and two near-infrared bands (NIR and Narrow NIR) of Sentinel-2 data were used. The Sentinel-2 bands at the 20-m spatial resolution were resampled to a 10-m spatial resolution by nearest-neighbor resampling (Louis et al., 2016). Finally, layer stacking, seamless mosaic, and subset were performed using the ENVI 5.3 software, and 22 images for classification were finally obtained. In ArcGIS, slope calculation was carried out on DEM data of Linxia County, and slope data of the study area were cut out. The categories of rural settlements in LUCC data in 2015, 2018, and 2020 were extracted respectively, and the data set of rural settlements in Linxia County during the study period was obtained by ArcGIS overlay analysis. Finally, buffer zones of 50, 100, and 200 m were constructed around the roads of Linxia County, and zones of 100, 200, and 500 m were constructed around the rural settlements. The purpose was to superimpose the abandoned cropland plots extracted (Section 3.3) to represent the influence range and degree of road and rural settlements on cropland abandonment.

3.2. Generation of the annual land use map

3.2.1. Image segmentation

Image segmentation is a key step in object-oriented image processing and determines the initial objects for subsequent processing and analysis. These objects are cluster pixels that can be separated from the surrounding objects and have a certain homogeneity. Here, we first generated the object by performing Multi-Resolution Segmentation (MRS) in eCognition (Baatz and Schape, 2000). Based on the homogeneity criterion, the algorithm combines pixels or image objects into a larger image object that has certain homogeneity and can be separated from the surrounding objects from the bottom up. When the object's attributes exceed the heterogeneity threshold defined by the segmentation scale, the growth of the object stops. After continuous optimization, the internal weighted heterogeneity of each object is minimized. The MRS is adjusted by using four key parameters, namely the scale parameter (SP), weights for compactness and smoothness, weights for

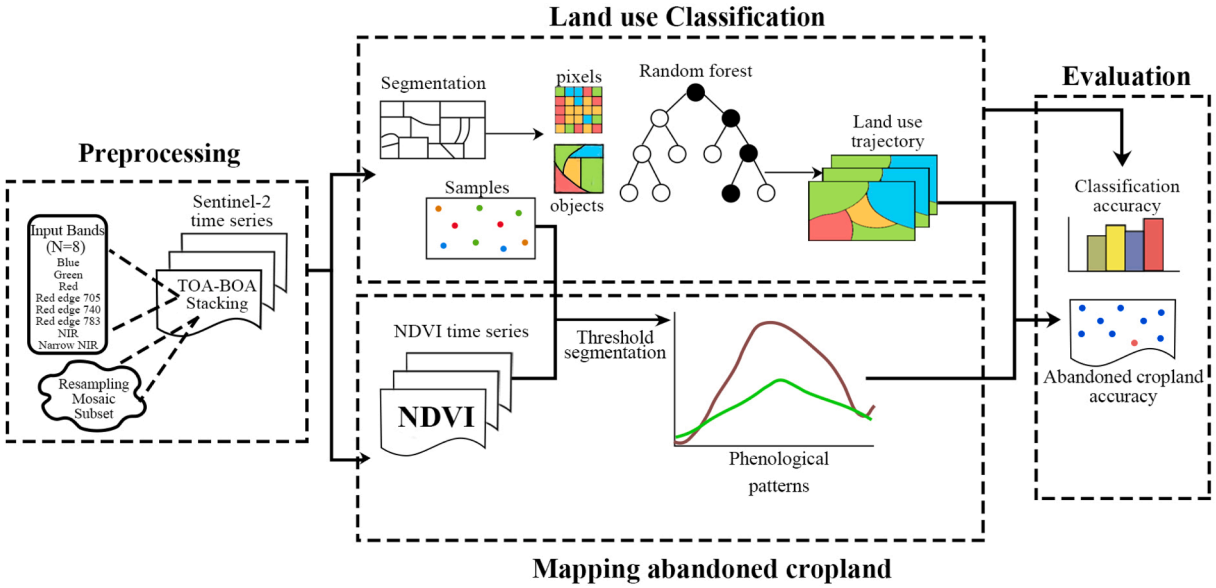

Fig. 2. Technical flow of mapping abandoned cropland.

color and shape, and band weights. In this study, all spectral bands were used, and the NIR bands were given higher weights for image segmentation (Johnson and Xie, 2011). The weights of compactness and smoothness as well as color and shape were obtained by using the control variable method to traverse trial and error and constantly adjust the parameters.

The scale parameter (SP) is the key control factor in the MRS and divides the whole image into different image objects. It controls the spectral heterogeneity of image objects; i.e., the larger the SP value, the greater the internal heterogeneity and the higher the number of pixels per image object (Johnson and Xie, 2011). Whilst comparing multiple segmentation results through user vision can flexibly incorporate expert knowledge into GEOBIA, it is limited by time, a high labor demand, and high costs (Duro et al., 2012; Arvor et al., 2013). On the other hand, different experts may have different ideas about the SP with the highest segmentation quality, making it highly subjective. Here, the SP was determined by optimal segmentation scale estimation (ESP2) (Dragut et al., 2014). In this method, the image is automatically segmented with a fixed increment of scale, and the homogenous local variance of the image object is calculated as the average standard deviation of the segmented object layer to determine the optimal segmentation scale. The optimal scale parameter of object segmentation is expressed by the rate of change (ROC) of local variance (LV). When the LV-ROC decreases and suddenly peaks, the corresponding segmentation scale is the optimal segmentation scale. The equation is as follows:

$$ROC = \frac{L_i - L_{i-1}}{L_{i-1}} \times 100\% \quad (1)$$

where ROC is the change rate of the corresponding LV, and L_i is the average standard deviation of the segmentation object at the i layer of the image.

Subsequently, the maximum area of the image object at different segmentation scales was calculated using the maximum area method (Huang, 2003). In object-oriented image analysis, the concept of resolution is replaced by the area of the image object (the product of the number of pixels that make up the object and the pixel resolution size). The maximum area of the image object can reflect the characteristics of the size change of the object with the segmentation scale. The segmented image is exported as a vector file, and the segmentation scale and the maximum area of the image object are, respectively, taken as the horizontal and vertical axes to draw the change curve of the maximum area of the image object with the segmentation scale. The curve platform corresponds to the range of the most suitable segmentation scale extracted from each category. Finally, the optimal segmentation scale was determined by the combination of ESP2 and the maximum area method.

3.2.2. Sample selection

According to the LUCC classification system of the Chinese Academy of Sciences and the actual situation of the study area, we divided the land use types into six typical categories: cropland, forest, grassland, water area, built-up land, and unused land. To train and validate the results of land use classification, we intersected the datasets over these 3 years and extracted plots that had remained unchanged for 3 years as a preliminary reference for sample selection. Second, to ensure that the classified sample data were distributed as evenly as possible in the entire study area, we used ArcGIS 10.5 to generate approximately 1,500 uniformly distributed random points within the study area. By comparing land use data, Google Earth images, and visual discrimination of Sentinel-2 images, random points that simultaneously met the three criteria were selected as sample points, and random points that did not meet these criteria were deleted. Overall,1,228 sample points were obtained. Of these, 860 sample points were selected for sample training of the random forest model, and the remaining 368 samples were used for accuracy validation of the classification results. Finally, the sample points are assigned to the polygonal blocks after segmentation, and the training and verification samples at the object level were obtained.

3.2.3. Feature Space construction

The initial feature space was constructed from four aspects: spectral feature, shape feature, texture feature, and spectral index feature.

Spectral feature: three visible bands (red, green, and blue), two near-infrared bands (NIR and Narrow NIR), and three unique red-edge bands (705, 740, and 783) of Sentinel-2 satellite were selected. The red-edge band is highly sensitive to the vegetation state, and within the range of the band, the vegetation reflectance rises sharply, making it an important indicator for vegetation classification and vegetation growth assessment (Thanh and Kappas, 2017, Sitokonstantinou et al., 2018). Mean and Standard deviation of the above eight bands, Brightness Settings (the sum of the number of layers of the image object divided by the mean of the layers containing spectral information), and maximum intra-object difference (Diff) were selected as the initial spectral feature set, with a total number of 18.

Texture features: In the early 1970 s, Haralick et al. (1973) proposed the gray-level co-occurrence matrix (GLCM). By calculating the probability of a direction θ separate step D gray value, we can extract the image spatial structure. Some studies show that adding the GLCM can improve the accuracy of remote sensing image classification (Marceau et al., 1990, Huang and Zhang, 2012). Here, GLCM Ang.2nd moment, GLCM Entropy, GLCM Contrast, GLCM StdDev, GLCM Correlation, GLCM Homogeneity, and GLCM Dissimilarity were selected. The statistical means of all directions were selected as the initial texture feature set, with a total of seven.

Shape feature: The image object layer generated after multi-resolution segmentation has an obvious shape feature, which can be used to improve the accuracy of image classification (Stumpf and Kerle, 2011). We selected border index, compactness, density, shape index, elliptic fit, roundness and rectangular asymmetry fit, area, length/width, and asymmetry as the initial shape feature set, with a total of 10.

Spectral index feature: After ratio processing, the spectral index can partially eliminate the influence of changes in irradiance conditions related to solar elevation angle, satellite observation angle, terrain, cloud/shadow, and atmospheric conditions (Carlson and Ripley, 1997). In this study, 9 representative spectral indices were selected as the initial classification feature set. The NDVI (Carlson and Ripley, 1997) can well represent the vegetation growth state and vegetation coverage and can effectively distinguish vegetation from soil and water. The ratio vegetation index (RVI) (Major et al., 1990) is more sensitive when monitoring high vegetation coverages and can better overcome the shortcomings of easy saturation in high-vegetation areas of the NDVI. The difference Vegetation Index (DVI) (Jiang et al., 2006) and the soil-adjusted vegetation index (SAVI) (Huete, 1988) can correct the sensitivity of the NDVI to soil background and overcome the disadvantage that the NDVI is easily affected by soil background in low-vegetation areas. As a sensitive vegetation band, the red edge can more effectively reflect the spectral characteristics of vegetation. Three red-edge normalized vegetation indices (NDVI R_{705}, NDVI R_{740}, and NDVI R_{783}) were constructed to participate in the classification (Clevers and Gitelson, 2013). The bareness Index (BI) (Chen et al., 2006) can reflect the bare condition of non-vegetation soil, whereas the normalized difference water index (NDWI) (Gao, 1996) can be used to highlight water information in the image.

This study used the Feature Space Optimization module in eCognition Developer 9.0 to select appropriate features. Based on the 44 features selected above, the feature separation function was constructed. Based on the samples of each category and the initial feature set, the

feature combination with the maximum average and minimum distance between the categories is the optimal feature collection of the classification. In this way, problems such as a sharp increase in calculation amount, a reduction in classification accuracy, and the redundancy of classification features caused by blindly using multiple features in the classification process can be avoided. In this study, when the feature dimension reached 31 dimensions, the category separability was highest; therefore, the optimal feature space was set as 31 dimensions (Supplementary Fig. 1, Table 2).

3.2.4. Random forest classification

The random forest classifier (RF) uses bootstrap bagging to search a random subspace from a given feature and optimal split nodes by minimizing the correlation between trees, resulting in an ensemble of trees. It can effectively describe the nonlinear relationship between the spectral characteristics of ground objects and their physical conditions and has the ability to resist noise and overfitting; it can therefore effectively deal with unbalanced data. Compared with other classifiers, RF is faster and easier to implement (Breiman, 2001; Tian et al., 2016). Precise land cover classification and better performance of RF models have been described previously (Pelletier et al., 2016; Sharma et al., 2016; Wessels et al., 2016). First, the selected training samples were assigned to the segmented image object, and second, RF in eCognition was used for classification. In this study, the eCognition software was used to set three parameters by default: Max categories were set to 16, Max tree number was set to 50, and Forest accuracy was set to 0.01. In similar studies, this parameter showed the best classification results (Husson et al., 2016; Oreti et al., 2021; Stefanski et al., 2013).

3.2.5. Accuracy assessment of land use classification

We used the producer accuracy (PA), user accuracy (UA), overall accuracy (OA), and Kappa coefficients to verify the land-use classification results in the confusion matrix. The PA is the ratio of correctly classified plots to the actual total number of plots on the ground, whereas UA is the ratio of correctly classified plots of land in a given category to the total number of plots predicted to fall into that category. The OA is the ratio of the number of correctly classified plots to the total number of plots (Story and Congalton, 1986). The statistical measure Kappa is used to describe the overall classification accuracy and is generally superior to simple accuracy measures because it accounts for the random agreement between authenticity and estimates (Cohen, 1960).

Table 2
The geographic object-based image classification object features.

Feature Set	Feature Description
Spectral feature	Mean values of red edge 740, red edge 783, NIR, Narrow NIR (4 variables) Standard deviation of blue, red, red edge 705, red edge 740, red edge 783, NIR, Narrow NIR (7 variables)
Vegetation index feature	NDVI (Carlson and Ripley, 1997), RVI (Major et al., 1990), NDVI R_{705}, NDVI R_{740}, NDVI R_{783} (Clevers and Gitelson, 2013), SAVI (Huete, 1988), NDWI (Gao, 1996) (7 variables)
Texture features	GLCM Entropy, GLCM StdDev, GLCM Correlation (3 variables)
Shape features	Border index, Compactness, Density, Shape Index, Elliptic Fit, Roundness, Rectangular Fit, Area, Length/Width, Asymmetry (10 variables)

Notes: NDVI (normalized difference vegetation index), the formula is (NIR −Red)/(NIR + Red). RVI (ratio vegetation index), the formula is NIR/R. NDVI R_{705} (normalized difference vegetation index red edge 705), the formula is (NIR −Red edge 705)/(NIR + Red edge 705). NDVI R_{740} (normalized difference vegetation index red edge 740), the formula is (NIR −Red edge 740)/(NIR + Red edge 740). NDVI R_{783} (normalized difference vegetation index red edge 783), the formula is (NIR −Red edge 783)/(NIR + Red edge 783). SAVI (soil-adjusted vegetation index), the formula is 1.5 × (NIR −Red)/(NIR + Red + 0.5). NDWI (normalized difference water index), the formula is (Green −NIR)/(Greeen + NIR).

3.3. Extraction of abandoned cropland Within-Year

3.3.1. Construction of the NDVI time series Within-Year

The NDVI time series dataset was constructed by analyzing the quarterly variation within-year. The year 2019 was taken as an example, the classified cropland boundary was extracted as a mask to establish the NDVI time series from April to October 2019, the harmonic analysis of time series method (Hants) (Zhang et al., 2014a) was used to smooth the NDVI time series, and the NDVI change map of the cropland in the study area in 2019 was obtained (Fig. 3).

The NDVI value of planted cropland was low in April, high in July, and decreased sharply in October; the overall change range was large, and fluctuation was violent. The NDVI decreased slightly at the end of April and increased again at the end of October, which may have been caused by weeding during the sowing period and grass growing after the harvesting period. In contrast, the change trend of the NDVI of abandoned cropland was different, and the change range of the NDVI was considerably smaller than that of planted cropland. From May to July, the NDVI slowly climbed to the maximum value, followed by a decrease after August. In general, the NDVI value of planted cropland in the study area in April was slightly lower than that of abandoned cropland, and the NDVI value in July considerably differed from that of abandoned cropland in July, with a sharp decrease in October, the NDVI value of planted cropland was lower than that of abandoned cropland. Based on this, the NDVI data for spring, summer, and autumn of 2018, 2020, and 2021 were generated by the ENVI software to enable the threshold division and distinction between planted and abandoned cropland.

3.3.2. Threshold segmentation

The main purpose of threshold segmentation is to compare the NDVI time series curves of planted and abandoned cropland within-year and find the best threshold that can distinguish the two. Otsu (Otsu, 1979) is an adaptive threshold segmentation algorithm proposed by the Japanese scholar Nobuyuki Otsu; it divides the image into target and background, based on its gray level. Finding the best segmentation threshold through traversal, achieving the largest variance among categories, or obtaining the smallest within-class variance, this algorithm is the most widely used algorithm of automatic segmentation threshold today. In this study, the selection of the segmentation threshold was mainly determined by the combination of the following points: comparing the optimal

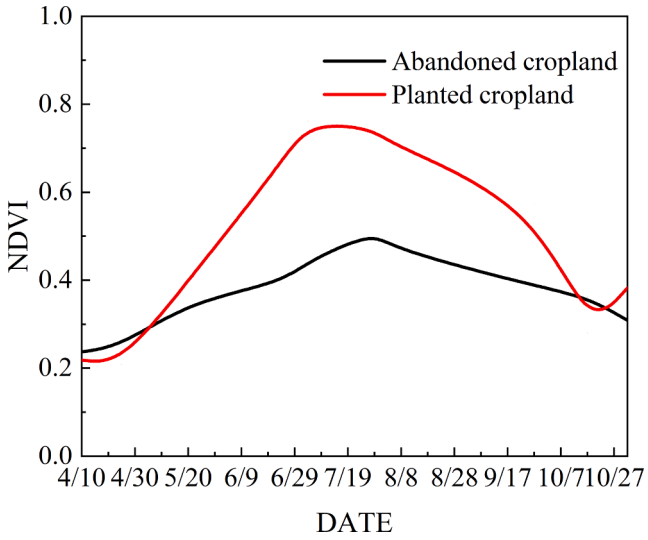

Fig. 3. NDVI changes in different categories of cropland in Linxia County from April to October 2019. NDVI = normalized difference vegetation index.

segmentation threshold calculated by Otsu with the NDVI change information of planted and abandoned cropland and using the feature view function provided by the eCognition Developer 9.0 software for repeated testing. Finally, the optimal threshold to distinguish planted from abandoned land was found, the planted land was extracted by eCognition threshold classification, and the abandoned cropland was extracted indirectly by subtracting the planted from the total cropland.

3.3.3. Defining and identifying the cropland type

In this study, referring to the definition of abandoned cropland by the European Union Environmental Policy Institute (Keenleyside et al., 2010), combined with the actual situation of the study area, the cropland that had not been planted for 2 consecutive years or more was classified as spontaneously abandoned cropland, and cropland that had not been cultivated for only 1 year was classified as fallow cropland. Abandonment caused by returning cropland to forest was classified as induced abandonment, and cropland occupied by built-up land was classified as lost cropland. Judging from the natural succession of vegetation coverage after cropland abandonment, in the initial stage, the original cropland was dominated by annual herbaceous species, with a sparse distribution. Over time, the proportion of these species gradually decreases, making room for perennial herbs, dwarf woody plants, or shrubs (Brown and Southwood, 1987; Alcantara et al., 2012). In the absence of human disturbance, the change from bare ground to a site with annual or perennial herbs can take 1 to 3 years, whereas dwarf woody plants or shrubs occur after 4 to 5 years and mature trees after at least 10 years (Smaliychuk et al., 2016; Nguyen et al., 2018). However, vegetation succession may be accelerated due to policy factors, such as the Chinese policy of returning cropland to forests and some grassland restoration programs in the United States, such as the Conservation Reserve Program (CRP) (Song and Pijanowski, 2014), which was launched in 1985. In such cases, new forests are formed within a shorter time after abandonment. Based on the above definition, we generated the cropland change trajectory from 2017 to 2021. First, the cropland boundary of the classified initial year was used to mask the study area, and the changes in the land use type of each object (T) in the initial range of cropland in other years were judged respectively. If T was cropland during the whole study period, the object was classified as stable cropland. If T was eventually replaced by built-up land, the object was classified as lost farmland. In case T was subjected to the transformation from cropland to grassland and then to woodland, the object was classified as induced abandoned land. If T was transformed from cropland to unused land or grassland, and the continuous period of unused land or grassland was more than 2 years, the object was classified as spontaneously abandoned. If T had not been cultivated within 1 year during the study period and was recultivated in other years, the object was classified as fallow cropland.

3.3.4. Extraction of abandoned cropland Within-Year

By using the cropland boundary obtained by classification as the limit range, we excluded the interference of changing ground objects outside the cropland range. Based on the seasonal differences in the NDVI between planted and abandoned cropland, two changes were detected from spring-summer and summer-autumn, and the two detection results were combined to extract the planted cropland within-year. We subtracted the planted cropland from the total cropland to obtain the unplanted cropland. Finally, we used the ArcGIS software to intersect these areas with the different types of cropland objects extracted from the annual land use trajectory, and the distinction of spontaneous abandonment, fallow, induced abandonment, and lost cropland was made. The equations used for extracting different cropland types were as follows:

$$A_S = A_U \cap T_S \tag{2}$$

$$A_F = A_U \cap T_F \tag{3}$$

$$A_I = A_U \cap T_I \tag{4}$$

$$A_L = A_U \cap T_L \tag{5}$$

$$A_U = C - D_1 \cup D_2, \tag{6}$$

where A_U is the range of uncultivated land in a certain year during the study period, A_S is the spontaneously abandoned cropland in a certain year during the study period, T_S is the spontaneously abandoned cropland extracted from the annual land use trajectory, and so on, A_F, A_I, A_L are fallow cropland, induced abandoned cropland, and lost cropland, respectively, during the study period, T_F, T_I, T_L are fallow cropland, induced abandoned cropland, and lost cropland extracted from the annual land use trajectory, respectively, C is the range of cropland in a certain year during the study period, D_1 is the detection result from spring to summer, and D_2 is the detection result from summer to autumn.

3.3.5. Accuracy assessment of abandoned cropland

Recall was used to verify the accuracy of the farmland abandonment map. In the ArcGIS software, 100 random sampling points were established annually on the plots of spontaneously abandoned cropland and fallow cropland extracted from 2018 to 2021, and 20 and 50 random sampling points were established annually on the plots of induced abandoned cropland and lost cropland, respectively. Minimum point spacing was 150 m. A visual assessment of Sentinel-2 image time series from 2018 to 2021 was used to verify actual land cover categories. To avoid misunderstandings caused by within-year changes in crop growth, Cloudless images collected in spring (April to May), summer (June to August), and autumn (October to November) were selected for interpretation (Prishchepov et al., 2012b; Yin et al., 2018b). A 0.49-m spatial resolution image from Google Earth was used to facilitate visual interpretation. Two experts then marked the plots where each point was located as positive or negative, i.e., correctly or incorrectly extracted abandoned cropland. When the two experts' assessments differed, a third expert was asked to mark the point in order to reach a majority decision. Using this validation dataset, we calculated the extraction accuracy of abandoned croplands using the following equation (Khurshid and Khan, 2014):

$$Recall = \frac{TP}{TP + FN} \times 100\% \tag{7}$$

where "*TP*" (true positive) indicates that the prediction is positive, that is, correctly extracted abandoned cropland, and "*FN*" (false negative) indicates that the prediction is negative, that is, incorrectly extracted abandoned cropland.

4. Results

4.1. Multiple resolution segmentation

In this study, the optimal level of MRS was obtained using the combination of ESP2 and the maximum area method, and the MRS Algorithm was run using weights of 0.1 for color and shape and 0.5 for compactness and smoothness. By testing the number of segmentation objects at different segmentation scales, the SP of 10 was the starting point, and the step size of 5 was used to segment the image. When the SP is small, the number of the segmented objects varies dramatically, and as the SP gradually increases, the change amplitude becomes extremely slow (Supplementary Fig. 2A). We chose SP 40 as the starting point of image segmentation scale selection and took SP 150 as the end point (Supplementary Fig. 2B). The step length was set to 5, and the number of cyclic segmentation times was set to 100. The above parameters were fed into ESP2, and the optimal segmentation scales identified were 71, 100, and 119, respectively (Supplementary Fig. 3). The parameters of

the maximum area method were set as above, the maximum area of the image object increased in the form of a ladder with the increase in the segmentation scale, and the platform periods with an unchanged middle area were 75–80, 90–95,100–105, and 125–130 (Supplementary Fig. 4), respectively. Combining ESP2 and maximum area methods, 100 was finally selected as the most appropriate SP for the image.

4.2. Land use classification

4.2.1. Land use classification accuracy

We used the object-based method to generate five different land use/cover maps of Linxia County for the period from 2017 to 2021 and used the confusion matrix to calculate the overall, producer, and user accuracy, respectively, with the aim to verify the accuracy of land cover types in Linxia County (Table 3). Although the accuracy of different

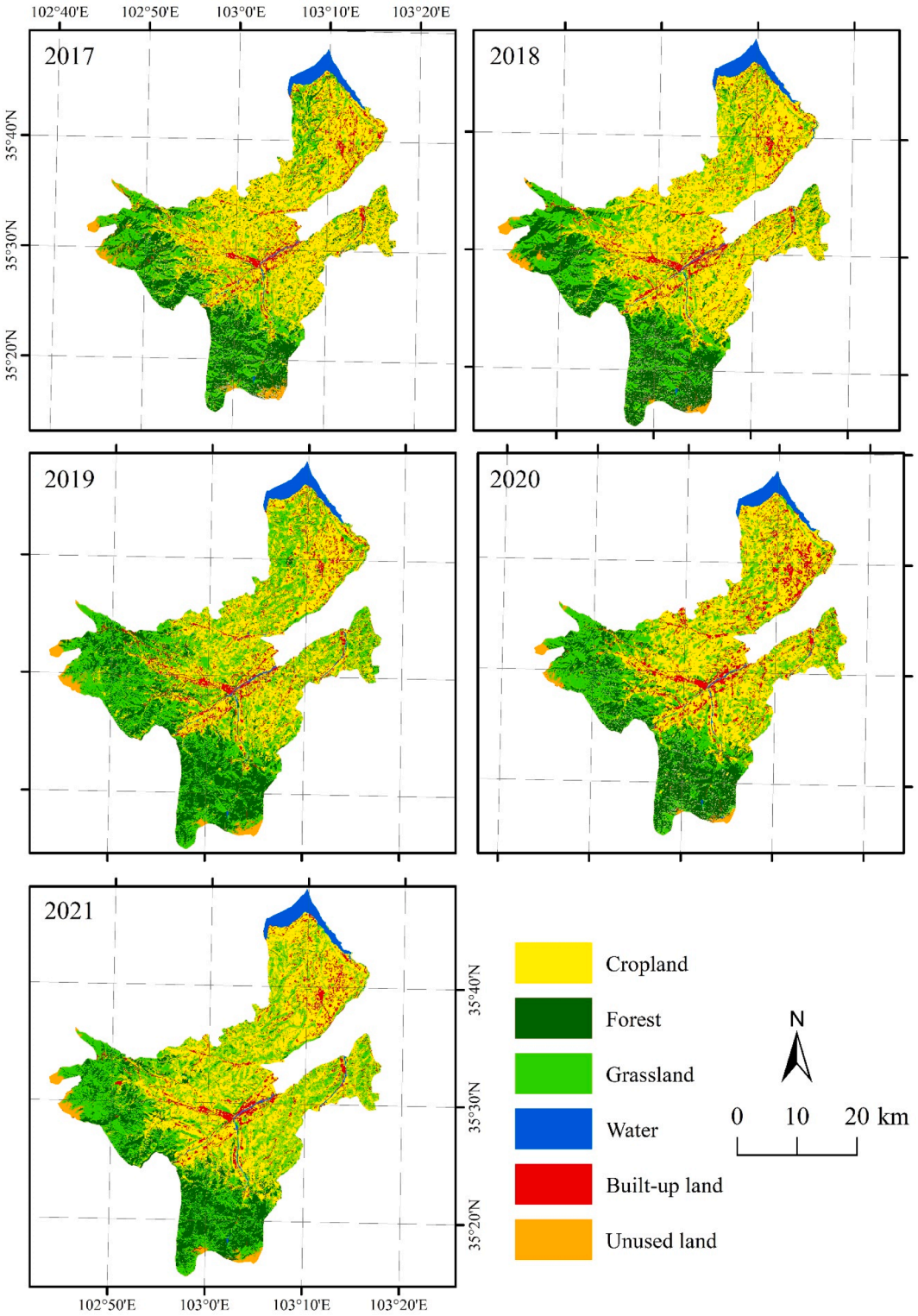

Fig. 4. Land use classification results for Linxia County from 2017 to 2021.

Table 3
Producer Accuracy (PA), User Accuracy (UA), Overall Accuracy (OA), and Kappa Coefficient for Linxia County from 2017 to 2021.

Type	2017		2018		2019		2020		2021	
	PA	UA	PA	UA	PA	UA	PA	UA	PA	UA
Cropland	0.98	0.99	0.99	0.97	0.87	0.84	0.96	0.95	0.93	0.89
Forest	1	0.98	0.98	0.98	0.92	0.97	0.96	0.98	0.96	0.9
Grassland	0.96	0.98	0.92	0.98	0.88	0.91	0.91	0.94	0.74	0.86
Water	1	1	1	1	0.9	0.69	1	1	1	1
Built-up land	1	0.92	1	0.9	0.71	0.77	0.97	0.97	1	0.94
Unused land	0.88	1	1	0.8	0.78	0.58	1	1	1	1
OA	0.98		0.97		0.87		0.95		0.89	
Kappa	0.97		0.96		0.83		0.93		0.84	

categories differed, that of our overall mapping was between 87 % and 98 %, the producer accuracy of cropland ranged between 87 % and 99 %, the user accuracy was between 84 % and 99 %, and the Kappa coefficient of the results of the five phases was greater than 0.8. This leads us to infer that the method is ideal for land use/cover types and can be used for the subsequent analysis of the land use change trajectory.

4.2.2. Land use change

Based on the land use map from 2017 to 2021 (Fig. 4), cropland in Linxia County was mainly distributed in the eastern and northern regions, whereas forest and grassland areas were more dominant in the western and southern areas. Over time, the cropland area showed a trend towards fragmentation. Built-up areas were distributed in the middle and northeast areas of Linxia County, on both sides of the river. With economic development, the built-up area increased slightly, mainly in the eastern and northern parts of the study area.

4.3. Distribution of abandoned cropland Within-Year

4.3.1. Abandoned cropland extraction accuracy

We used Sentinel-2 time series and Google Earth images to verify the extraction accuracy for different cropland types in Linxia County from 2018 to 2021. The recall of spontaneously abandoned cropland ranged from 79 % to 82 %, and that of fallow cropland was slightly lower, from 71 % to 76 %, mainly due to confusion between these two categories. The recall values of induced abandoned cropland and lost cropland were high, and the 4-year average annual recall values were 91.25 % and 89.5 %, respectively (Table 4).

4.3.2. Extraction results of abandoned cropland Within-Year

According to our method, cropland abandoned in Linxia County from 2018 to 2021 was extracted (2017 was taken as the initial year, not included in the cropland type statistics) (Fig. 5). From 2018 to 2021, significant cropland abandonment occurred in the central, eastern, and northern regions of the study area. Fig. 6 shows the statistics of the different cropland types. From 2018 to 2021, the spontaneous abandonment rate in Linxia County ranged between 7.70 % and 15.80 %; this abandonment type was most pronounced in 2019, with an area of 28.97 km^2. The fallow rates ranged between 5.11 % and 16.76 %, with the highest fallow area of 30.72 km^2 in 2019. Both induced abandoned cropland and lost cropland reached maximum values 2021, accounting for 1.75 % and 7.19 %, respectively, with areas of 3.80 and 15.58 km^2, respectively. Based on these findings, cropland abandonment in Linxia County peaked in 2019.

4.4. Analysis of the spatial change characteristics of abandoned cropland

Generally, spontaneously abandoned cropland is located in mountainous areas with higher slopes or near road networks; the reasons for abandonment are usually socioeconomic, ecological, or political factors (Song and Deng, 2017; Næss et al., 2021). In addition, labor migration leads to an increase in abandoned cropland in emigration areas (Li and Tan, 2018). In this study, we selected slope, distance from the road network, and distance from rural settlements to study their effects on spontaneous cropland abandonment.

4.4.1. Slope

By calculating the abandonment rates of different types of plots under each slope (Fig. 7), we found that with increasing slope, cropland abandonment generally became more pronounced. In 2018 and 2020, the relationship between slope and abandonment rate was first positive and then negative, which was more pronounced at slopes greater than 24°, where the area of cropland decreased sharply, resulting the abandonment rate under the slope decreased slightly.

4.4.2. Distance from the road network

As seen in Fig. 8, the distance from the road network greatly impacted cropland abandonment. The area of abandoned cropland within 50–100 m from the road network was smallest, and with increasing distance to the road, cropland abandonment was more pronounced.

4.4.3. Distance from rural settlements

According to Fig. 9, cropland abandonment was clearly related to the distance from rural settlements. Within the range of 100–200 m from rural settlements, the abandonment rate was low, indicating that this distance is more suitable for farmers to cultivate their land. Cropland too far or too close to rural settlements was more likely to be abandoned.

Table 4
Accuracy of the assessment of abandoned cropland in Linxia County from 2018 to 2021.

	SA			FL			IA			LC		
	TP	FN	Recall	TP	FN	Recall	TP	FN	Recall	TP	FN	Recall
2018	81	19	81 %	74	26	74 %	20	0	100 %	46	4	92 %
2019	81	19	81 %	76	24	76 %	17	3	85 %	45	5	90 %
2020	79	21	79 %	73	27	73 %	18	2	90 %	45	5	90 %
2021	82	18	82 %	71	29	71 %	18	2	90 %	43	7	86 %

Notes: SA: spontaneously abandoned cropland, FL: fallow cropland, IA: induced abandoned cropland, LC: lost cropland, TP: “true positive”, FN: “false negative”.

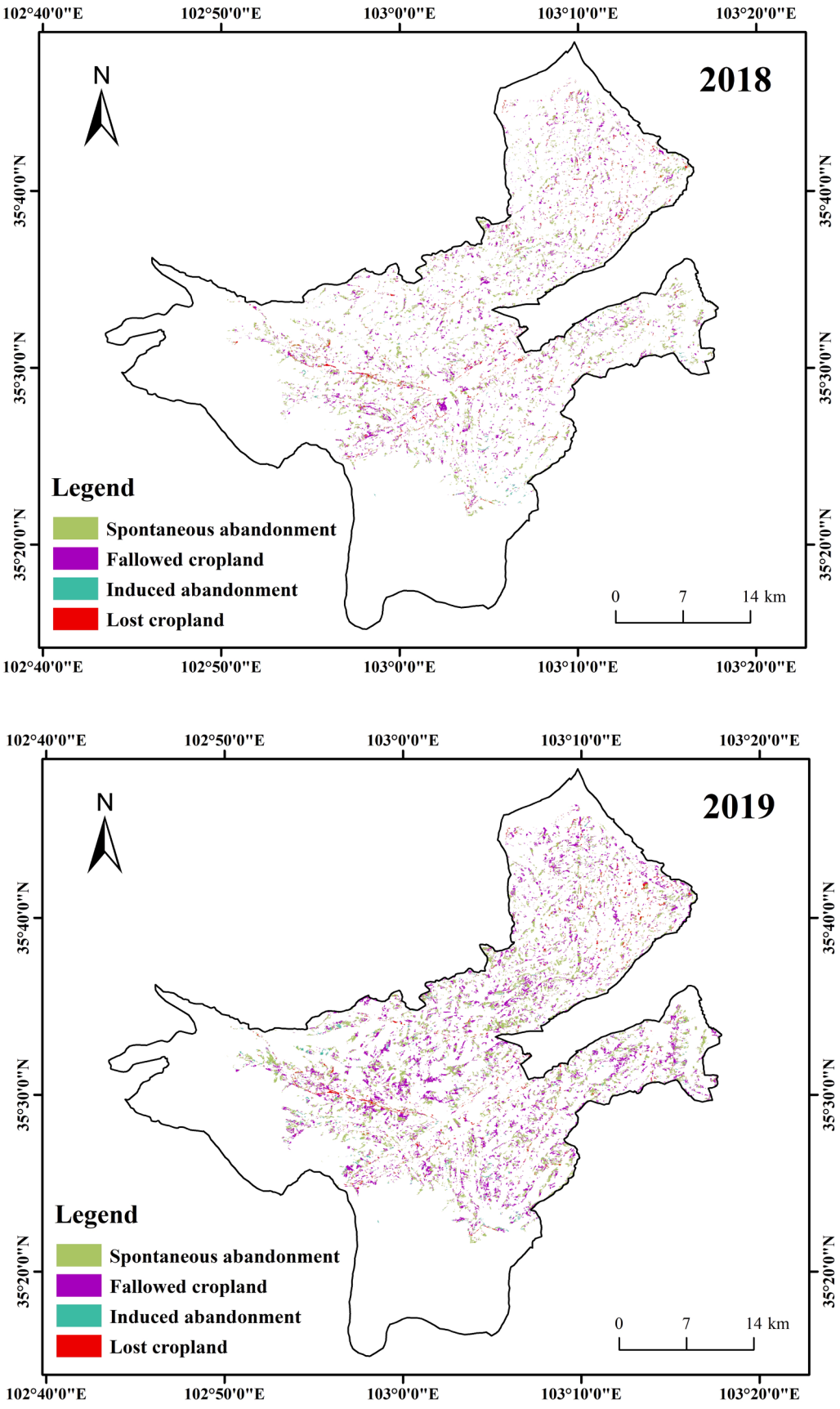

Fig. 5. Distribution of different abandoned cropland types in Linxia County from 2018 to 2021.

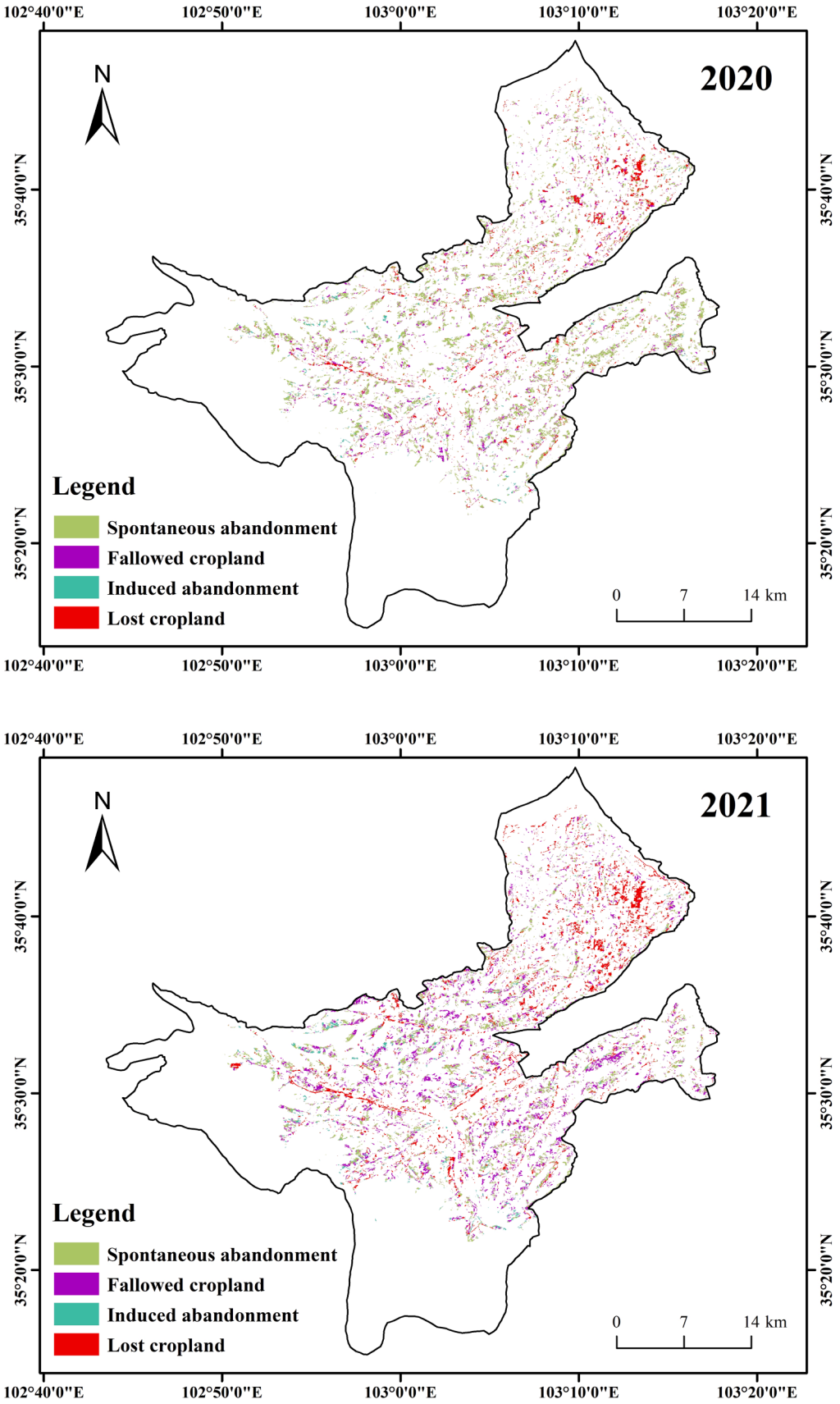

Fig. 5. (*continued*).

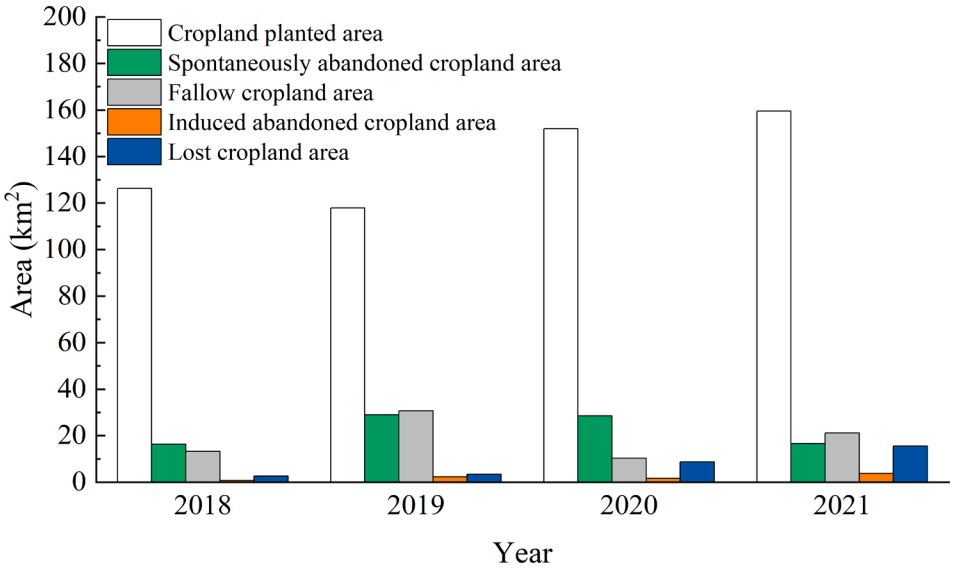

Fig. 6. Statistics of cropland types in Linxia County from 2018 to 2021.

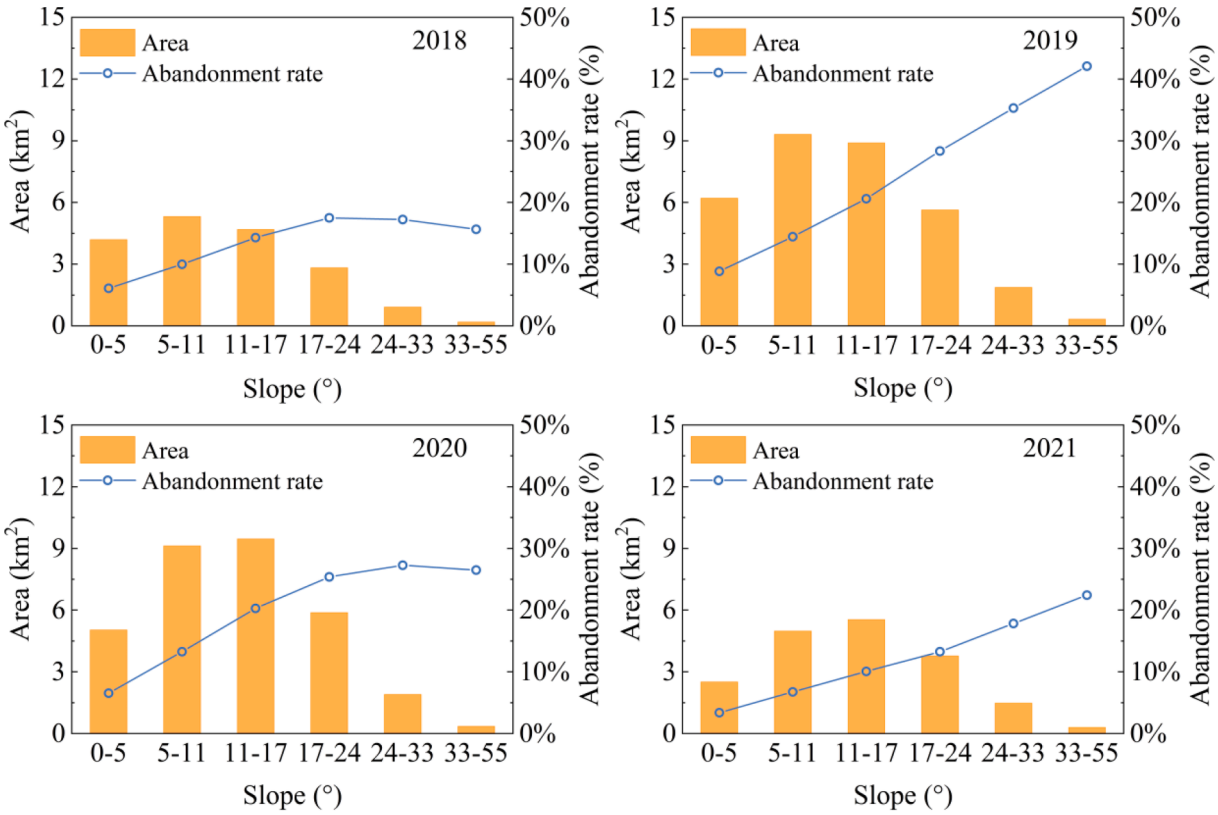

Fig. 7. Spontaneous cropland abandonment rates under different slopes in Linxia County from 2018 to 2021.

5. Discussion

5.1. Object-oriented classification

In previous studies on abandoned cropland, the pixel level was the dominant level (Pueyo and Beguería, 2007; Prishchepov et al., 2012a, 2013; Lasanta et al., 2017). Here, Sentinel-2 images were segmented, and the object was taken as the basic unit for monitoring abandoned cropland. The main advantages are as follows: 1) Object-oriented image analysis technology delineated polygonal plots closer to real cropland characteristics through image segmentation, which could be directly stored and linked to the database as attributes or features, thus facilitating managers to directly guide and formulate policies on cropland abandonment in a given region (Ming et al., 2015; Gil-Yepes et al., 2016). 2) By eliminating the "salt-and-pepper effect" caused by pixel-level classification, inadequate classifications of abandoned cropland caused by mixed pixels were avoided, and the error transmission caused by classification accuracy in the extraction of abandoned cropland by the trajectory of land use was reduced, thus achieving a higher detection accuracy (Yin et al., 2018b). 3) Spatial segmentation reduces intra-class

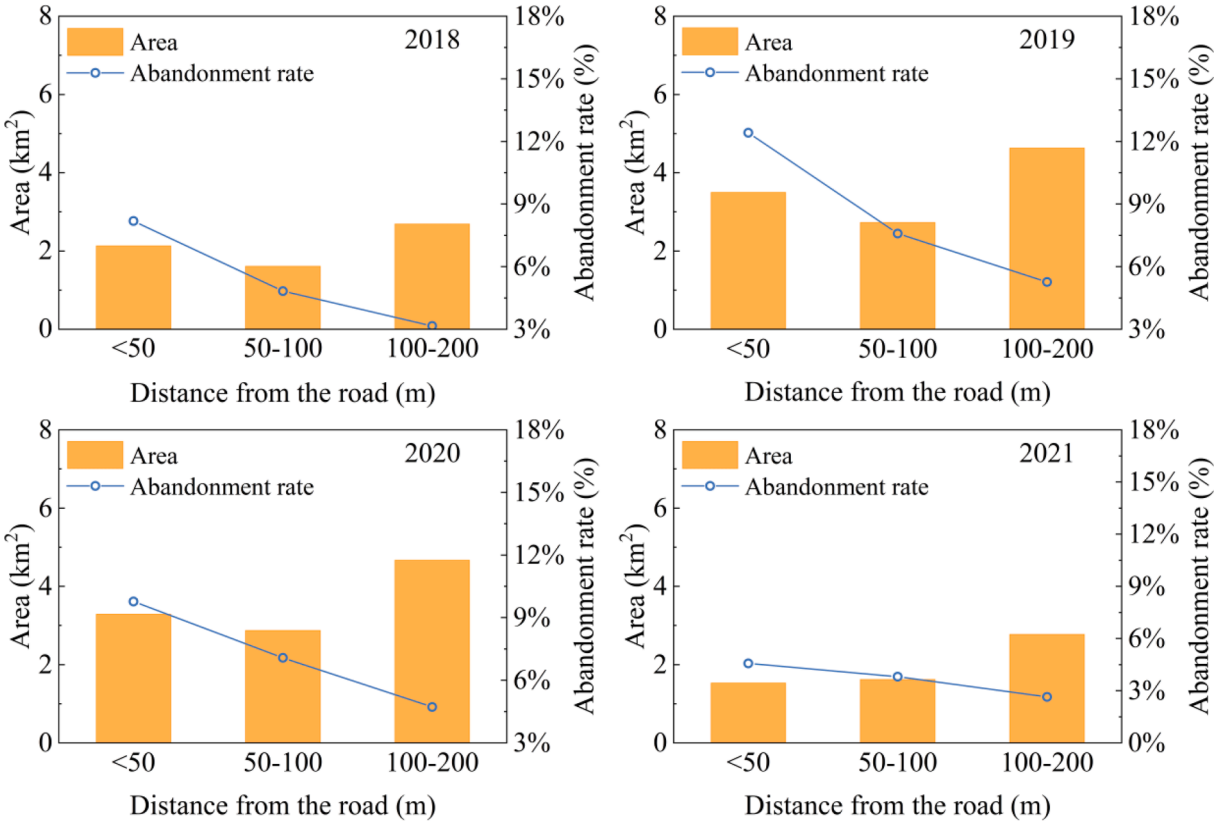

Fig. 8. Spontaneous cropland abandonment rate as a factor of distance to the road in Linxia County from 2018 to 2021.

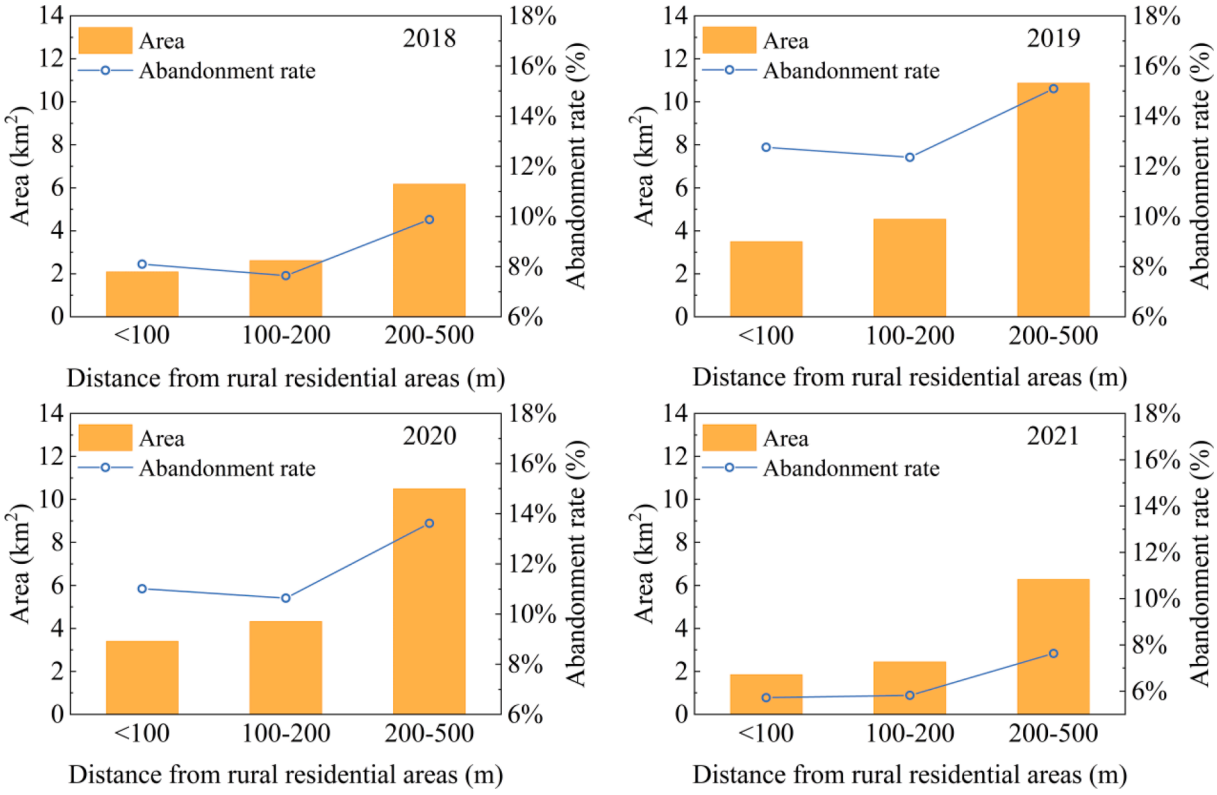

Fig. 9. Spontaneous cropland abandonment rate as a factor of distance to rural settlements in Linxia County from 2018 to 2021.

spectral heterogeneity by dividing the image into relatively uniform areas, effectively using Sentinel-2′s high spatial resolution and neighborhood information, such as size, shape, texture, and topological relations (Benz et al., 2004; Blaschke, 2010; Johnson and Xie, 2011).

Image segmentation is a challenge in object orientation because it requires user intervention to define the best segmentation parameters for describing objects of interest (Belgiu and Csillik, 2018). To determine the optimal segmentation scale parameters, we used the optimal segmentation scale estimation (ESP2) combined with the maximum area method to control the internal heterogeneity of objects, which is more labor-, time-, and cost-efficient. Notably, multi- resolution segmentation can achieve top-down or bottom-up segmentation of different object scales by creating multiple levels. The main purpose of this study was to extract cropland boundaries, and only one of the hierarchies was selected for segmentation. If the goal is to identify the actual crop or other plant types, further refinement is required (Oreti et al., 2021).

5.2. Comparisons with previous studies

Our work uses Sentinel-2 images to extract abandoned cropland. Compared with the plots of abandoned cropland based on Landsat annual time series (Prishchepov et al., 2012b; Kraemer et al., 2015; Song, 2019), high spatial resolution enables us to successfully identify the boundaries of fragmented cropland in mountainous areas and reduce underestimating the abandoned cropland area. A high time resolution throughout the year allows us to map changes in different vegetation types throughout the growth cycle, which is especially important when monitoring abandoned cropland (Alcantara et al., 2013; Estel et al., 2015). Moreover, the original image was subjected to orthographic correction and subpixel level geometric precision correction, and the image after 2019 was subjected to atmospheric correction; this approach saves time and costs. We also applied the vegetation red edge bands (705, 740, and 783) specially used for cropland mapping in the classification process, which showed high values in the feature construction, consistent with previous findings (Immitzer et al., 2016).

The abandoned cropland within-year was extracted by threshold segmentation and subsequently combined with the interannual dynamic database obtained from the land use trajectory. The complementarity of the two methods was used to reduce the extraction errors; simultaneously, different cropland types within-year could be easily distinguished, which alleviated the pressure of manpower to identify heavy sample databases. The reliability of our method was tested by comparison with other relevant studies in mountainous areas of China. For example, Shi et al. (2018) obtained the distribution map of abandoned cropland from 2002 to 2011 by superimposing two phases of cultivated map layers in typical counties in Chongqing, China, for 2002 and 2011, obtaining abandonment rates between 15 % and 20 %. Li et al. (2017) conducted a sample survey on cropland abandonment in mountainous areas and counties in China and calculated an average abandonment rate of 14.32 %. The cropland abandonment rate extracted by our method was 13.03 %, which is consistent with the result of Li et al. (2017) and is slightly lower than that of Shi et al. (2018); this discrepancy is likely a result of the spatial pattern of cropland abandonment in mountainous areas of China, which is high in the south and low in the north (Li et al., 2017). Alcantara et al. (2012) adopted the MODIS NDVI time series product and combined it with support vector machine classification to monitor abandoned cropland in the Baltic States, Belarus, and Poland, obtaining an accuracy rate of 65 %. Based on the annual map of active cropland and non-cropland areas in 14 regions of the world from 1987 to 2017, Yin et al. (2020) extracted abandoned cropland by analyzing the land-use trajectories of each pixel, with an identification accuracy of approximately 75 %. The accuracy rate of our method was approximately 81 %, slightly higher than that of the study mentioned above.

5.3. Method transferability

We used Sentinel-2 satellite images to identify abandoned cropland. These open-source data cover the entire world and are freely available, which can be extended to other parts of the world. We tested our method in a mountainous area of China (Linxia County), and our findings were consistent with the characteristics of cropland fragmentation in mountainous areas. We used the EU Environmental Policy Institute's definition of cropland abandonment (i.e., cessation of farming for more than 2 years), which is the same as the local government department's definition of cropland abandonment (Linxia County People's Government Network, 2022b). This implies that our method can be used to map cropland abandonment in other parts of China and of the world with similar land-use change processes. However, adjustments may be needed before applying our approach directly to other areas with different social and natural environments. Due to differences in climate, soil conditions, and agricultural policies in different regions, the fallow periods may exceed 5 years in some areas (Rudel et al., 2009; Estel et al., 2015). In this case, other satellite images (such as the Landsat series), with earlier launch time and longer operating time, should be selected, and in the selection of segmentation scale parameters, changes in image spatial resolution may need to be considered. When the study area is shifted to a larger scale, a pixel may contain multiple land use types, and pixel or subpixel analysis should be preferred (Blaschke, 2010). In addition, the temporal resolution of Landsat data is not high, and some areas of individual images are easily covered by clouds; in this case, it may not be possible to construct NDVI time series changing with the growth cycle of vegetation. On these grounds, multi-source remote sensing data should be combined to complete the research. Our method can also be applied to other land use change studies, such as crop classification (Immitzer et al. 2016; Belgiu and Csillik, 2018), urban building and road identification (Myint et al. 2011), forest mapping (Conchedda et al., 2008), and wetland monitoring (Dronova et al., 2011).

5.4. Suggestions on the reclamation of abandoned cropland in Linxia County

From 2018 to 2021, approximately 13.03 % of the cropland in Linxia County, Gansu Province, was abandoned yearly. Among the four cropland types, spontaneously abandoned cropland was relatively densely distributed in the plain area of Linxia County, accounting for the highest proportion (11.98 %) of abandoned cropland. For example, in areas with a slope below 24°, the average annual area of spontaneously abandoned cropland was 23.34 km^2, accounting for approximately 93 % of the abandoned cropland in this area. We estimated the production potential of this part of abandoned cropland of Linxia County using the cropland production potential data of the Chinese Academy of Sciences (RESDC, 2017). Based on the results, if all these abandoned cropland sites can be reclaimed, the local grain production can be increased by 5,147.7 tons, accounting for 3.6 % of the county's total grain output in 2021 (Linxia County People's Government Network, 2022a). However, reclamation needs to be combined with information on the local physical geography and human activities. Since 2003, agricultural labor costs in China have been increasingly rapidly (Zhang et al., 2014b; Fang et al., 2009), and farmers usually take mechanical measures as alternative to labor to cope with the loss of profits caused by rising labor costs. However, in some of the more remote areas, the lack of transportation has hindered the mechanization of agriculture, cropland reclamation in such areas requires more labor and management input (MacDonald et al., 2000; Strijker, 2005; Raj Khanal and Watanabe, 2006). Our analysis of the distance between abandoned cropland and rural settlements showed that the optimal distance of cropland to rural settlements is 100–200 (also referred to as the Euclidean distance, considering the impact of the terrain, and the actual distance is farther). Previous research has shown that farmers have shifted from mere food production to high-value

farming systems based on livestock and dairy production to increase their incomes. For example, the construction of dairy factories, slaughterhouses, and shared freezers near residential areas occupy cropland (Dixon et al., 2001; Pretty 2008). The reclamation of abandoned cropland sites that are far away may be more expensive because of the long distance to be travelled and inconvenient transportation (MacDonald et al., 2000). In recent years, the price of agricultural means of production continued to increase as an effect of a low farming efficiency. Numerous rural laborers sought employment outside the farm, and those living close to roads had more opportunities to find jobs in the non-farm sector (Khanal and Watanabe, 2006), which led to a shortage of agricultural laborers near the road network (Hatna and Bakker, 2011). The lack of labor force may further impede the reclamation of abandoned cropland. Therefore, we suggest that for abandoned cropland sites with small slopes and moderate traffic conditions, the management department should organize reclamation as soon as possible and give priority to their use for food production. Regarding abandoned sites due to outmigration, the farmland contractor or collective organization should be urged to transfer such sites to large farmers or cooperatives for reclamation and planting within a certain time limit. In the case of abandoned farmland because of inconvenient transportation, it is necessary to improve the farmland infrastructure conditions through the construction of mechanical cultivation roads and other measures. In the unstable and vulnerable global food security landscape, policymakers can introduce a series of subsidies for land and food prices to encourage local farmers to reclaim their cropland in these moderate areas.

6. Conclusions

Based on high-resolution Sentinel-2 time-series data, this study used an object-oriented method and RF to draw a land use map of Linxia County from 2017 to 2021. Abandoned cropland was extracted from 2018 to 2021 via intra-annual change detection, and four cropland types were determined: spontaneously abandoned cropland, induced abandoned cropland, fallow cropland, and lost cropland. The overall accuracy of land use classification was 89 %–98 %, and the average annual extraction accuracies for spontaneously and induced abandoned cropland were 81 % and 91 %, respectively, which confirms the reliability of our method. We also analyzed the spatial and temporal changes of abandoned cropland to study the influence mechanisms of slope, traffic, and other factors on the reclamation of abandoned cropland.

From 2018 to 2021, the average spontaneous abandonment rate in Linxia County was 11.98 %, with the highest value in 2019. Spontaneously abandoned cropland accounted for the largest proportion, followed by fallow, lost, and induced abandoned cropland. Most of the abandoned cropland was located in areas with relatively moderate quality, and cropland abandonment was highest in areas close to roads and far from rural residential areas. The reclamation of abandoned cropland of moderate quality can increase the local grain yield by 3.6 %. The method proposed in this study may be applied to map abandoned cropland in other areas or in other land use mapping studies.

Data Availability Statement.

The majority of the datasets used in this study are publicly available and can be accessed through public repositories. All used data repositories are cited either in the main text.

The remote sensing image data includes 44 periods of Sentinel-2A/B satellite images with cloud cover less than 20 % from April 2017 to November 2021 in Linxia County, Gansu Province, China. Data from European Space Agency. This website allows real name applications. The Google Earth Image with a spatial resolution of 0.49 m was used to assess the accuracy of the land-use classification and abandoned cropland maps. Data from 91 Weitu Assistant (https://www.91weitu.com/).

The 2015, 2018 and 2020 remote sensing datasets of land use and land cover in Linxia County, which were used as a reference for delineating samples and rural settlements in the research were obtained from the Resources and Environmental Sciences and Data Center, Chinese Academy of Sciences (https://www.resdc.cn/).

The GDEMV3 30 M resolution digital elevation model data in Linxia County, Gansu Province, China comes from the Geospatial Data Cloud site (https://www.gscloud.cn/). This website allows real name applications.

Road network vector data in Linxia County, Gansu Province, China comes from Open street map (https://master.apis.dev.openstreetmap.org/). This website allows real name applications.

A dataset of farmland productivity potential in China comes from Resource and Environment Science and Data Center (https://www.resdc.cn/). This website allows real name applications.

Declaration of Competing Interest

The authors declare that they have no known competing financial interests or personal relationships that could have appeared to influence the work reported in this paper.

Data availability

I have explained the data availability in the manuscript

Acknowledgments

This research was supported by the Project of National Natural Science Foundation of China (grant number 42071233), the Second Tibetan Plateau Scientific Expedition and Research (grant number 2019QZKK0603), and the Strategic Priority Research Program of Chinese Academy of Sciences (grant number XDA20040201).

References

Alcantara, C., et al., 2013. Mapping the extent of abandoned farmland in Central and Eastern Europe using MODIS time series satellite data. Environ. Res. Lett. 8, 035035.
Alcantara, C., Kuemmerle, T., Prishchepov, A.V., Radeloff, V.C., 2012. Mapping abandoned agriculture with multi-temporal MODIS satellite data. Remote Sens. Environ. 124, 334–347.
Alexander, P., et al., 2015. Drivers for global agricultural land use change: the nexus of diet, population, yield and bioenergy. Glob. Environ. Chang. 35, 138–147.
Arvor, D., Durieux, L., Andrés, S., Laporte, M.-A., 2013. Advances in Geographic Object-Based Image Analysis with ontologies: A review of main contributions and limitations from a remote sensing perspective. ISPRS J. Photogramm. Remote Sens. 82, 125–137.
Baatz, M., Schape, A., 2000. Multiresolution segmentation: an optimization approach for high quality multi-scale image segmentation. Beiträge zum. AGIT-Symposium.
Battude, M., et al., 2016. Estimating maize biomass and yield over large areas using high spatial and temporal resolution Sentinel-2 like remote sensing data. Remote Sens. Environ. 184, 668–681.
Baumann, M., et al., 2011. Patterns and drivers of post-socialist farmland abandonment in Western Ukraine. Land Use Policy 28, 552–562.
Belgiu, M., Csillik, O., 2018. Sentinel-2 cropland mapping using pixel-based and object-based time-weighted dynamic time warping analysis. Remote Sens. Environ. 204, 509–523.
Benz, U.C., Hofmann, P., Willhauck, G., Lingenfelder, I., Heynen, M., 2004. Multi-resolution, object-oriented fuzzy analysis of remote sensing data for GIS-ready information. ISPRS J. Photogramm. Remote Sens. 58, 239–258.
Blair, D., Shackleton, C.M., Mograbi, P.J., 2018. Cropland abandonment in South African smallholder communal lands: Land cover change (1950–2010) and farmer perceptions of contributing factors. Land 7, 121.
Blaschke, T., 2010. Object based image analysis for remote sensing. ISPRS J. Photogramm. Remote Sens. 65, 2–16.
Breiman, L., 2001. Random forests. Machine learning 45, 5–32.
V.K, Brown, T, Southwood, Secondary succession: patterns and strategies, Symposium of the British Ecological Society 1987.
Campbell, J.E., Lobell, D.B., Genova, R.C., Field, C.B., 2008. The global potential of bioenergy on abandoned agriculture lands. Environ. Sci. Tech. 42, 5791–5794.
Carducci, B., et al., 2021. Food systems, diets and nutrition in the wake of COVID-19. Nature Food 2, 68–70.
Carlson, T.N., Ripley, D.A., 1997. On the relation between NDVI, fractional vegetation cover, and leaf area index. Remote Sens. Environ. 62, 241–252.
Chen, X.-L., Zhao, H.-M., Li, P.-X., Yin, Z.-Y., 2006. Remote sensing image-based analysis of the relationship between urban heat island and land use/cover changes. Remote Sens. Environ. 104, 133–146.
Clevers, J.G.P.W., Gitelson, A.A., 2013. Remote estimation of crop and grass chlorophyll and nitrogen content using red-edge bands on Sentinel-2 and -3. Int. J. Appl. Earth Obs. Geoinf. 23, 344–351.

Cohen, J., 1960. A coefficient of agreement for nominal scales. Educ. Psychol. Meas. 20, 37–46.
Conchedda, G., Durieux, L., Mayaux, P., 2008. An object-based method for mapping and change analysis in mangrove ecosystems. ISPRS J. Photogramm. Remote Sens. 63, 578–589.
Dara, A., et al., 2018. Mapping the timing of cropland abandonment and recultivation in northern Kazakhstan using annual Landsat time series. Remote Sens. Environ. 213, 49–60.
Dasgupta, S., Robinson, E.J., 2022. Impact of COVID-19 on food insecurity using multiple waves of high frequency household surveys. Sci. Rep. 12, 1–15.
DeVries, B., et al., 2015. Tracking disturbance-regrowth dynamics in tropical forests using structural change detection and Landsat time series. Remote Sens. Environ. 169, 320–334.
V.d.T, di Caracalla, The impacts on global food security and nutrition of the military conflict in Ukraine 2022.
Dixon, J.A., Gibbon, D.P., Gulliver, A., 2001. Farming systems and poverty: improving farmers' livelihoods in a changing world. Food & Agriculture Org.
Dragut, L., Csillik, O., Eisank, C., Tiede, D., 2014. Automated parameterisation for multi-scale image segmentation on multiple layers. ISPRS J. Photogramm. Remote Sens. 88, 119–127.
Dronova, I., Gong, P., Wang, L., 2011. Object-based analysis and change detection of major wetland cover types and their classification uncertainty during the low water period at Poyang Lake, China. Remote Sens. Environ. 115, 3220–3236.
Drusch, M., et al., 2012. Sentinel-2: ESA's optical high-resolution mission for GMES operational services. Remote Sens. Environ. 120, 25–36.
Duro, D.C., Franklin, S.E., Dubé, M.G., 2012. A comparison of pixel-based and object-based image analysis with selected machine learning algorithms for the classification of agricultural landscapes using SPOT-5 HRG imagery. Remote Sens. Environ. 118, 259–272.
Duveiller, G., Defourny, P., 2010. A conceptual framework to define the spatial resolution requirements for agricultural monitoring using remote sensing. Remote Sens. Environ. 114, 2637–2650.
ESA (European Space Agency), 2021. Sentinel-2 data set in Linxia County. https://scihub.copernicus.eu/dhus/ (accessed 29 October 2021).
Estel, S., et al., 2015. Mapping farmland abandonment and recultivation across Europe using MODIS NDVI time series. Remote Sens. Environ. 163, 312–325.
Image Elevation Download Expert, 2021. The Google Earth Image in Linxia County. China (in Chinese). https://www.91weitu.com/ (accessed 10 February 2022).
C, Fang, D, Yang, W, Meiyan, Migration and labor mobility in China 2009.
Feizizadeh, B., Garajeh, M.K., Blaschke, T., Lakes, T., 2021. An object based image analysis applied for volcanic and glacial landforms mapping in Sahand Mountain. Iran. Catena 198, 105073.
Field, J.L., et al., 2020. Robust paths to net greenhouse gas mitigation and negative emissions via advanced biofuels. Proc Natl Acad Sci U S A 117, 21968–21977.
G, Fischer, M, Shah, H, Velthuizen, F., Nachtergaele, Agro-ecological zones assessments. Land use and land cover. Encyclopedia of Life Support Systems (EOLSS), Developed under the Auspices of the UNESCO. Eolss Publishers Oxford 2006.
Gao, B.-C., 1996. NDWI—A normalized difference water index for remote sensing of vegetation liquid water from space. Remote Sens. Environ. 58, 257–266.
GDC (Geospatial Data Cloud site, Computer Network Information Center, Chinese Academy of Sciences), 2021. GDEMV3 30M resolution digital elevation model data in Linxia County. http://www.gscloud.cn/ (accessed 14 April 2022).
Gelfand, I., et al., 2013. Sustainable bioenergy production from marginal lands in the US Midwest. Nature 493, 514–517.
Gil-Yepes, J.L., Ruiz, L.A., Recio, J.A., Balaguer-Beser, Á., Hermosilla, T., 2016. Description and validation of a new set of object-based temporal geostatistical features for land-use/land-cover change detection. ISPRS J. Photogramm. Remote Sens. 121, 77–91.
Haralick, R.M., Shanmugam, K., Dinstein, I.H., 1973. Textural features for image classification. IEEE Trans. Syst. Man Cybern. 610–621.
Hartvigsen, M., 2014. Land reform and land fragmentation in Central and Eastern Europe. Land Use Policy 36, 330–341.
Hatna, E., Bakker, M.M., 2011. Abandonment and expansion of arable land in Europe. Ecosystems 14, 720–731.
He, S., et al., 2022. Monitoring Cropland Abandonment in Hilly Areas with Sentinel-1 and Sentinel-2 Timeseries. Remote Sens. (Basel) 14, 3806.
Herrmann, I., et al., 2011. LAI assessment of wheat and potato crops by VENμS and Sentinel-2 bands. Remote Sens. Environ. 115, 2141–2151.
Huang, X., Zhang, L., 2012. An SVM ensemble approach combining spectral, structural, and semantic features for the classification of high-resolution remotely sensed imagery. IEEE Trans. Geosci. Remote Sens. 51, 257–272.
H, Huang, Research on Scale Problems in Object-Oriented Image Analysis Ph.D., Graduate School of Chinese Academy of Sciences (Institute of Remote Sensing Applications). China (in Chinese) 2003.
Huete, A.R., 1988. A soil-adjusted vegetation index (SAVI). Remote Sens. Environ. 25, 295–309.
Husson, E., Ecke, F., Reese, H., 2016. Comparison of manual mapping and automated object-based image analysis of non-submerged aquatic vegetation from very-high-resolution UAS images. Remote Sens. (Basel) 8, 724.
HWSD (Harmonized World Soil Database), 2009. Soil Units in the Revised Legend of the Soil Map of the World. https://www.fao.org/soils-portal/soil-survey/soil-maps-and-databases/harmonized-world-soil-database-v12/en/ (accessed 7 October 2022).
Im, J., Jensen, J., Tullis, J., 2008. Object-based change detection using correlation image analysis and image segmentation. Int. J. Remote Sens. 29, 399–423.
Immitzer, M., Vuolo, F., Atzberger, C., 2016. First experience with Sentinel-2 data for crop and tree species classifications in central Europe. Remote Sens. (Basel) 8, 166.
Inglada, J., et al., 2015. Assessment of an operational system for crop type map production using high temporal and spatial resolution satellite optical imagery. Remote Sens. (Basel) 7, 12356–12379.
Janowski, L., Kubacka, M., Pydyn, A., Popek, M., Gajewski, L., 2021. From acoustics to underwater archaeology: Deep investigation of a shallow lake using high-resolution hydroacoustics—The case of Lake Lednica, Poland. Archaeometry 63, 1059–1080.
Jiang, Z., et al., 2006. Analysis of NDVI and scaled difference vegetation index retrievals of vegetation fraction. Remote Sens. Environ. 101, 366–378.
Jin, Z., et al., 2019. Smallholder maize area and yield mapping at national scales with Google Earth Engine. Remote Sens. Environ. 228, 115–128.
Johnson, B., Xie, Z., 2011. Unsupervised image segmentation evaluation and refinement using a multi-scale approach. ISPRS Journal of Photogrammetry and Remote Sensing, 66(4), 473–483. ISPRS J. Photogramm. Remote Sens. 66, 473–483.
Keenleyside, C., Tucker, G., McConville, A., 2010. Farmland Abandonment in the EU: an Assessment of Trends and Prospects. Institute for European Environmental Policy, London.
Kehoe, L., et al., 2017. Biodiversity at risk under future cropland expansion and intensification. Nat Ecol Evol 1, 1129–1135.
Khanal, N.R., Watanabe, T., 2006. Abandonment of agricultural land and its consequences. Mt. Res. Dev. 26, 32–40.
Khurshid, H., Khan, M.F., 2014. Segmentation and classification using logistic regression in remote sensing imagery. IEEE J. Sel. Top. Appl. Earth Obs. Remote Sens. 8, 224–232.
Kim, J., et al., 2016. Low-dielectric-constant polyimide aerogel composite films with low water uptake. Polym. J. 48, 829–834.
Kraemer, R., et al., 2015. Long-term agricultural land-cover change and potential for cropland expansion in the former Virgin Lands area of Kazakhstan. Environ. Res. Lett. 10, 054012.
Kuemmerle, T., et al., 2013. Challenges and opportunities in mapping land use intensity globally. EconStor Open Access Articles and Book Chapters.
Kuntz, K.A., Beaudry, F., Porter, K.L., 2018. Farmers' perceptions of agricultural land abandonment in rural western New York State. Land 7, 128.
Lasanta, T., et al., 2017. Space–time process and drivers of land abandonment in Europe. Catena 149, 810–823.
Lebourgeois, V., et al., 2017. A combined random forest and OBIA classification scheme for mapping smallholder agriculture at different nomenclature levels using multisource data (simulated Sentinel-2 time series, VHRS and DEM). Remote Sens. (Basel) 9, 259.
Li, S., et al., 2017. Extent and distribution of cropland abandonment in Chinese mountainous areas. Resources Science 39, 1801–1811.
Li, W., Tan, M., 2018. Influences of vertical differences in population emigration on mountainous vegetation greenness: a case study in the Taihang Mountains. Sci. Rep. 8, 16954.
Li, Z., Yan, J., Hua, X., Xin, L., Li, X., 2014. Factors influencing the cultivated land abandonment of households of different types: a case study of 12 typical villages in Chongqing Municipality. Geogr. Res. 33, 721–734.
Linxia County People's Government Network, 2021. Announcement on the special rectification of abandoned cropland in Linxia County. China (in Chinese). http://www.linxiaxian.gov.cn/ (accessed 13 May 2022).
Linxia County People's Government Network, 2022a. Statistical bulletin of national economic and social development of Linxia County in 2021. China (in Chinese). http://www.linxiaxian.gov.cn/ (accessed 10 June 2022).
Linxia County People's Government Network, 2022b. Linxia County made solid progress in the special rehabilitation of abandoned cropland. China (in Chinese). http://www.linxiaxian.gov.cn/ (accessed 9 November 2022).
Linxia Hui Autonomous Prefecture People's Government Network, 2021. Our prefecture has completed the 200000 Mu project of returning cropland to forest and grassland. China (in Chinese). http://www.linxia.gov.cn/ (accessed 13 May 2022).
Liu, J., et al., 2014. Spatiotemporal characteristics, patterns, and causes of land-use changes in China since the late 1980s. J. Geog. Sci. 24, 195–210.
Liu, L., Xu, X., Chen, X., 2015. Assessing the impact of urban expansion on potential crop yield in China during 1990–2010. Food Security 7, 33–43.
Louis, J., et al., 2016. Sentinel-2 Sen2Cor: L2A processor for users, Proceedings Living Planet Symposium 2016. Spacebooks Online 1–8.
MacDonald, D., et al., 2000. Agricultural abandonment in mountain areas of Europe: environmental consequences and policy response. J. Environ. Manage. 59, 47–69.
Major, D., Baret, F., Guyot, G., 1990. A ratio vegetation index adjusted for soil brightness. Int. J. Remote Sens. 11, 727–740.
Marceau, D.J., Howarth, P.J., Dubois, J.-M.-M., Gratton, D.J., 1990. Evaluation of the grey-level co-occurrence matrix method for land-cover classification using SPOT imagery. IEEE Trans. Geosci. Remote Sens. 28, 513–519.
Matton, N., et al., 2015. An automated method for annual cropland mapping along the season for various globally-distributed agrosystems using high spatial and temporal resolution time series. Remote Sens. (Basel) 7, 13208–13232.
Miller, D.C., Muñoz-Mora, J.C., Christiaensen, L., 2017. Prevalence, economic contribution, and determinants of trees on farms across Sub-Saharan Africa. Forest Policy Econ. 84, 47–61.
Ming, D., Li, J., Wang, J., Zhang, M., 2015. Scale parameter selection by spatial statistics for GeOBIA: Using mean-shift based multi-scale segmentation as an example. ISPRS J. Photogramm. Remote Sens. 106, 28–41.
U, Muller-Wilm, J, Louis, R, Richter, F, Gascon, M, Niezette, Sentinel-2 level 2A prototype processor: Architecture, algorithms and first results, Proceedings of the ESA Living Planet Symposium, Edinburgh, UK 2013, pp. 9-13.
Myint, S.W., Gober, P., Brazel, A., Grossman-Clarke, S., Weng, Q., 2011. Per-pixel vs. object-based classification of urban land cover extraction using high spatial resolution imagery. Remote Sens. Environ. 115, 1145–1161.

Næss, J.S., Cavalett, O., Cherubini, F., 2021. The land–energy–water nexus of global bioenergy potentials from abandoned cropland. Nat. Sustainability 4, 525–536.
Nguyen, H., Hölzel, N., Völker, A., Kamp, J., 2018. Patterns and determinants of post-Soviet cropland abandonment in the Western Siberian Grain Belt. Remote Sens. (Basel) 10, 1973.
Oreti, L., Giuliarelli, D., Tomao, A., Barbati, A., 2021. Object oriented classification for mapping mixed and pure forest stands using very-high resolution imagery. Remote Sens. (Basel) 13, 2508.
OSM (Open Street Map), 2021. Road network vector data in Linxia County. https://master.apis.dev.openstreetmap.org/ (accessed 26 April 2022).
Otsu, N., 1979. A threshold selection method from gray-level histograms. IEEE Trans. Syst. Man Cybern. 9, 62–66.
Pelletier, C., Valero, S., Inglada, J., Champion, N., Dedieu, G., 2016. Assessing the robustness of Random Forests to map land cover with high resolution satellite image time series over large areas. Remote Sens. Environ. 187, 156–168.
Pörtner, L.M., et al., 2022. We need a food system transformation—In the face of the Russia-Ukraine war, now more than ever. One. Earth.
Pretty, J., 2008. Agricultural sustainability: concepts, principles and evidence. Philos. Trans. R. Soc., B 363, 447–465.
Prishchepov, A.V., Radeloff, V.C., Baumann, M., Kuemmerle, T., Müller, D., 2012a. Effects of institutional changes on land use: agricultural land abandonment during the transition from state-command to market-driven economies in post-Soviet Eastern Europe. Environ. Res. Lett. 7, 024021.
Prishchepov, A.V., Radeloff, V.C., Dubinin, M., Alcantara, C., 2012b. The effect of Landsat ETM/ETM+ image acquisition dates on the detection of agricultural land abandonment in Eastern Europe. Remote Sens. Environ. 126, 195–209.
Prishchepov, A.V., Müller, D., Dubinin, M., Baumann, M., Radeloff, V.C., 2013. Determinants of agricultural land abandonment in post-Soviet European Russia. Land Use Policy 30, 873–884.
Pueyo, Y., Beguería, S., 2007. Modelling the rate of secondary succession after farmland abandonment in a Mediterranean mountain area. Landsc. Urban Plan. 83, 245–254.
Raj Khanal, N., Watanabe, T., 2006. Abandonment of agricultural land and its consequences: a case study in the Sikles area. Gandaki Basin, Nepal Himalaya.
RESDC (Resource and Environment Science and Data Center), 2017. A dataset of farmland productivity potential in China. https://www.resdc.cn/ (accessed 30 May 2022).
RESDC (Resource and Environment Science and Data Center), 2020. Remote sensing monitoring data of land use status in Linxia County, Gansu Province, China in 2015, 2018, and 2020. https://www.resdc.cn/ (accessed 3 November 2021).
Romero-Calcerrada, R., Perry, G.L., 2004. The role of land abandonment in landscape dynamics in the SPA 'Encinares del río Alberche y Cofio, Central Spain, 1984–1999. Landsc. Urban Plan. 66, 217–232.
Rudel, T.K., et al., 2009. Agricultural intensification and changes in cultivated areas, 1970–2005. Proc. Natl. Acad. Sci. 106, 20675–20680.
Schierhorn, F., et al., 2013. Post-Soviet cropland abandonment and carbon sequestration in European Russia, Ukraine, and Belarus. Global Biogeochem. Cycles 27, 1175–1185.
Sharma, R.C., Tateishi, R., Hara, K., Iizuka, K., 2016. Production of the Japan 30-m land cover map of 2013–2015 using a Random Forests-based feature optimization approach. Remote Sens. (Basel) 8, 429.
Shi, T., Li, X., Xin, L., Xu, X., 2018. The spatial distribution of farmland abandonment and its influential factors at the township level: a case study in the mountainous area of China. Land Use Policy 70, 510–520.
Siebert, S., Portmann, F.T., Döll, P., 2010. Global patterns of cropland use intensity. Remote Sens. (Basel) 2, 1625–1643.
Sitokonstantinou, V., et al., 2018. Scalable parcel-based crop identification scheme using Sentinel-2 data time-series for the monitoring of the common agricultural policy. Remote Sens. (Basel) 10, 911.
Smaliychuk, A., et al., 2016. Recultivation of abandoned agricultural lands in Ukraine: Patterns and drivers. Glob. Environ. Chang. 38, 70–81.
SNAP (Sentinels Application Platform), 2019. European Space Agency. http://step.esa.int/main/download/snap-download/ (accessed 29 Otcober 2021).
Song, W., 2019. Mapping cropland abandonment in mountainous areas using an annual land-use trajectory approach. Sustainability 11, 5951.
Song, W., Deng, X., 2017. Land-use/land-cover change and ecosystem service provision in China. Sci. Total Environ. 576, 705–719.
Song, W., Pijanowski, B.C., 2014. The effects of China's cultivated land balance program on potential land productivity at a national scale. Appl. Geogr. 46, 158–170.
Stefanski, J., Mack, B., Waske, B., 2013. Optimization of object-based image analysis with random forests for land cover mapping. IEEE J. Sel. Top. Appl. Earth Obs. Remote Sens. 6, 2492–2504.
Story, M., Congalton, R.G., 1986. Accuracy assessment: a user's perspective. Photogramm. Eng. Remote Sens. 52, 397–399.
Stow, D., Hamada, Y., Coulter, L., Anguelova, Z., 2008. Monitoring shrubland habitat changes through object-based change identification with airborne multispectral imagery. Remote Sens. Environ. 112, 1051–1061.
Strijker, D., 2005. Marginal lands in Europe—causes of decline. Basic Appl. Ecol. 6, 99–106.
Stumpf, A., Kerle, N., 2011. Object-oriented mapping of landslides using Random Forests. Remote Sens. Environ. 115, 2564–2577.
Thanh Noi, P., Kappas, M., 2017. Comparison of random forest, k-nearest neighbor, and support vector machine classifiers for land cover classification using Sentinel-2 imagery. Sensors 18, 18.
Tian, S., Zhang, X., Tian, J., Sun, Q., 2016. Random forest classification of wetland landcovers from multi-sensor data in the arid region of Xinjiang. China. Remote Sensing 8, 954.
Tilman, D., Balzer, C., Hill, J., Befort, B.L., 2011. Global food demand and the sustainable intensification of agriculture. Proc. Natl. Acad. Sci. 108, 20260–20264.
Tilman, D., Clark, M., 2014. Global diets link environmental sustainability and human health. Nature 515, 518–522.
Tollefson, J., 2022. What the war in Ukraine means for energy, climate and food. Nature 604, 232–233.
Valero, S., et al., 2016. Production of a dynamic cropland mask by processing remote sensing image series at high temporal and spatial resolutions. Remote Sens. (Basel) 8, 55.
Van Tricht, K., Gobin, A., Gilliams, S., Piccard, I., 2018. Synergistic Use of Radar Sentinel-1 and Optical Sentinel-2 Imagery for Crop Mapping: A Case Study for Belgium. Remote Sens. (Basel) 10.
Wang, Y., Song, W., 2021. Mapping Abandoned Cropland Changes in the Hilly and Gully Region of the Loess Plateau in China. Land 10.
Wessels, K.J., et al., 2016. Rapid land cover map updates using change detection and robust random forest classifiers. Remote Sens. (Basel) 8, 888.
Whiteside, T.G., Boggs, G.S., Maier, S.W., 2011. Comparing object-based and pixel-based classifications for mapping savannas. Int. J. Appl. Earth Obs. Geoinf. 13, 884–893.
Xiong, J., et al., 2017. Nominal 30-m Cropland Extent Map of Continental Africa by Integrating Pixel-Based and Object-Based Algorithms Using Sentinel-2 and Landsat-8 Data on Google Earth Engine. Remote Sens. (Basel) 9.
Yan, J., et al., 2016. Drivers of cropland abandonment in mountainous areas: A household decision model on farming scale in Southwest China. Land Use Policy 57, 459–469.
Yin, H., et al., 2018b. Mapping agricultural land abandonment from spatial and temporal segmentation of Landsat time series. Remote Sens. Environ. 210, 12–24.
Yin, H., et al., 2020. Monitoring cropland abandonment with Landsat time series. Remote Sens. Environ. 246.
Yin, H., Pflugmacher, D., Li, A., Li, Z., Hostert, P., 2018a. Land use and land cover change in Inner Mongolia-understanding the effects of China's re-vegetation programs. Remote Sens. Environ. 204, 918–930.
Zhang, Y., Li, X., Song, W., 2014b. Determinants of cropland abandonment at the parcel, household and village levels in mountain areas of China: A multi-level analysis. Land Use Policy 41, 186–192.
Zhang, Q., Xiao, M., Singh, V.P., Chen, Y.D., 2014a. Max-stable based evaluation of impacts of climate indices on extreme precipitation processes across the Poyang Lake basin, China. Global Planet. Change 122, 271–281.
Zumkehr, A., Campbell, J., 2013. Historical US cropland areas and the potential for bioenergy production on abandoned croplands. Environ. Sci. Tech. 47, 3840–3847.